Environmental Modelling and Software 173 (2024) 105936

Contents lists available at ScienceDirect

Environmental Modelling and Software

journal homepage: www.elsevier.com/locate/envsoft

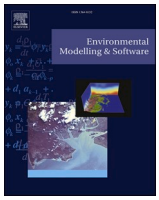

Evaluation of surrogate flood models for the use in impact-based flood warning systems at national scale

Markus Mosimann [a,b,c,*], Martina Kauzlaric [a,b,c], Simon Schick [a,b,c], Olivia Martius [a,b,c], Andreas Paul Zischg [a,b,c]

[a] Institute of Geography, University of Bern, Hallerstrasse 12, 3012, Bern, Switzerland
[b] Mobiliar Lab for Natural Risks, University of Bern, Hallerstrasse 12, 3012, Bern, Switzerland
[c] Oeschger Centre for Climate Change Research, University of Bern, Hochschulstrasse 4, 3012, Bern, Switzerland

ARTICLE INFO

Handling Editor: Daniel P Ames

Keywords:
Impact-based warning
Impact forecast
Surrogate flood model
Library-based surrogate model
Near real-time warning
Flood warning system

ABSTRACT

Recent flood events show that gaps in the communication channels from warning services to target groups inhibit mitigation. One approach addressing this issue is impact-based warning. We introduce a library-based surrogate flood model for the use in impact-based warning systems, tested for the main river network of Northern Switzerland. To validate the surrogate model, we compare the impacts to buildings, persons and workplaces with hazard classification, estimated with transient simulations for nine extreme precipitation scenarios. With 78 analyzed model regions, the surrogate approach reaches a Flood Area Index between 0.74 and 0.90 for each scenario (overall 0.84). The Critical Success Index calculated based on exposed persons is 0.77–0.93 (overall 0.89). Our prototype of a library-based flood surrogate model demonstrates the ability of accurately representing a same resolved transient model, bearing the potential to predict flood impacts nationwide in near real-time and the applicability to probabilistic forecasts.

1. Introduction

The European floods during summer 2021, the floods in Pakistan 2022 and the floods in California 2023 have once more demonstrated the destructive potential of floods and that they not only lead to high monetary damage but also cost many lives. Fekete and Sandholz (2021) take up the discussions that came up in Germany, after the European Floods 2021 revealed critical issues in disaster management. As one key to bridge communication gaps in future events, they recommend searching for solutions to "decode communication […] to better understand diverging and ambiguous information and interpretations". Besides the flood event in Germany, there are numerous examples globally where forecasts of upcoming natural hazards resulted in a poor response (World Meteorological Organization 2015). Considering that extreme weather- and climate-related events are projected to become generally more frequent and intense with climate change (Intergovernmental Panel on Climate Change, 2012), it becomes even more relevant to support decision makers in disaster management with appropriate warnings of natural hazards.

The World Meteorological Organization (WMO) published "Guidelines on Multi-hazard Impact-based Forecast and Warning Services" (World Meteorological Organization 2015), to support authorities with introducing warning systems that warn users of the possible consequences of a predicted extreme event. This concept is called impact-based warnings (IBWs) and impact forecasts (IFs). Additionally, increasing the availability of and giving access to early warning systems is one of the main targets given by the *Sendai Framework for Disaster Risk Reduction 2015–2030* (United Nations 2015). According to the WMO guidelines, IBWs inform target users about impacts that are expected due to the hazard of a forecasted weather event and known vulnerability, whereas IFs are defined as the "next evolutionary step of warnings" by adding explicit information about exposure on an individual or community level. This information should support their decisions on what mitigation measures to undertake next. Thus, IBWs and IFs aim at optimizing short-term prevention and risk management actions and are therefore issued in a specific way for each target group.

In recent years, the effectiveness of IBWs and IFs has been demonstrated repeatedly. IBWs have a significant effect on the intended

* Corresponding author. Institute of Geography, University of Bern, Hallerstrasse 12, 3012, Bern, Switzerland.
E-mail addresses: markus.mosimann@unibe.ch (M. Mosimann), martina.kauzlaric@unibe.ch (M. Kauzlaric), olivia.romppainen@unibe.ch (O. Martius), andreas.zischg@unibe.ch (A.P. Zischg).

https://doi.org/10.1016/j.envsoft.2023.105936
Received 3 March 2023; Received in revised form 15 December 2023; Accepted 15 December 2023
Available online 20 December 2023

response to an extreme event and together with behavioral recommendations they can improve the perception and the understanding of warnings (Weyrich et al., 2018). IBWs demonstrated to improve not only intended response but also risk perception (Potter et al., 2021). Compared to general warnings, IBWs increase the likelihood that protective decisions are taken (Meléndez-Landaverde et al., 2020; Casteel 2016, 2018). There is a clear need for improvements in collecting and storing flood impact data, as well as for describing or discussing technical standards (Kaltenberger et al., 2020; Potter et al., 2021).

Aiming at providing the highest level of flood warnings by means of highly resolved inundation models that are reliably informing about hazard and impact at a single house level is linked with high computational costs. Conversely, a suitable model for near-real time warnings on a national level needs to simulate predictions with enough lead time and substantially before the upstream element in the model chain gets updated. Therefore, we search for a flood modelling framework applicable as national warning system (Switzerland), optimizing the trade-off between computational efficiency and high resolution.

As model chains for flood risk assessment do not focus on computational efficiency or a coarse spatial resolution has to be selected, they do not fit the requirements for being implemented in IBW and IF frameworks (van Dyck et al., 2013; Ward et al., 2013; Falter et al., 2015; Foudi et al., 2015; Moncoulon et al., 2014; Alfieri et al., 2016; Felder et al., 2018). Recently, the potential for near-real time applications for large regions of highly resolved (10m) raster-based flood models running on GPU was shown (Ming et al., 2020; Apel et al., 2022). Besides that mainly hazard and not impact is in the focus of these studies, the resolution is still too coarse to correctly consider important hydraulic features like dikes, walls or flood defenses in rivers and floodplains. Although sub-grid approaches, or synonymously 1D-2D coupled models, allow to precisely embed river channel geometry into a 2D grid, these approaches show similar resolution-performance trade-offs as the ones used in flood risk assessment (Neal et al. 2011, 2012, 2015; Russo et al., 2015). As an alternative to inundation models running on regular, raster-based computational grids, the resolution of irregular meshes can be adapted for separate regions in the same model. In addition, the representation of hydraulic structures can be enforced when present in the underlying, highly resolved digital elevation model (Horritt and Bates 2002; Zischg et al., 2018b).

One approach to deal with the trade-off between computational time and spatial resolution are flood surrogate models (Zischg et al., 2018a), or synonymously called « flood libraries » or « flood impact libraries » when combined with exposure and physical vulnerability. These surrogate models are widely known and already applied especially in context of surface water floods (synonymously pluvial floods or flash floods) (Bermúdez et al., 2018; Aldridge et al., 2020; Cox et al., 2021). The term « flood libraries » comes from pre-calculated flood simulations that are stored in a database. In case of a flood forecast, the early warning system searches for the preprocessed flood simulation in the database for which the input hydrograph is similar to the forecasted hydrograph, here in terms of peak discharge. Surrogate modeling aims at developing "cheaper-to-run" surrogates of the original simulation models (Razavi et al., 2012). Surrogate models can be derived from computationally expensive models either by response surface modeling or by developing lower-fidelity models with simplified implementations of the physical equations. Response surface surrogate models and library-based surrogate models are also referred to as metamodels or a model of a model (Razavi et al., 2012). The term surrogate model is also used in the context of deep learning models replacing numerical simulations, an upcoming topic in the field of flood modelling.

To our knowledge, an application of surrogate flood models in IBWs and IFs of fluvial floods on a national scale has not been discussed yet and there is no general architecture or technical specification given defining requirements of a flood model for being a valid application for IBW and IF systems. Based on an analysis of extreme floods in the north alpine part of Switzerland, the goal of this study is to evaluate the potential and limitations of high-resolution flood surrogate models for IBWs or IFs on a national level and to discuss application opportunities, uncertainties and further needs for possible target users.

In this study, we focus on the loss of information when using precomputed flood scenarios (i.e., flood surrogate models) compared to transient simulations. For the model evaluation, we consider flood hazard as well as affected population and buildings.

2. Data and methods

To analyze and discuss the potential of flood surrogate models for an operationalization in impact-based flood warning systems, meteorological and hydrological uncertainties must be decoupled. We use synthetic hydrographs over a range of peaks specific for each floodplain to model flood and impact based on a spatially and temporally highly resolved flood model and store results as flood libraries in a database. The scenarios in the database can be identified by the name of the floodplain and the peak discharge of the used synthetic hydrographs. The nearest neighbor to the peak discharge of the hydrometeorological scenarios is then used as the basis for the prediction of the surrogate model. We use nine extreme hydrometeorological scenarios from reforecast archives as test cases for modelling the flood impacts. The hydrographs of these scenarios serve as input into transient flood models based on the same computational grid of the surrogate flood model. These are our benchmarks against which the surrogate models are compared. We measure the information loss on flood hazard and impact when using the flood surrogate models in comparison to the results of the transient simulation.

2.1. Study area

Fig. 1 gives an overview of the study area. We consider 24 Swiss rivers together with Lake Lucerne, Lake Thun, Lake Walen and Lake Brienz. The study area covers a relevant part of the main headwater catchments of Northern Switzerland, covering parts of the Swiss Plateau, the Jura mountains, alpine Prealps and the northern Alpine ridge. There are river sections with lakes as upstream boundary conditions: the Aare River downstream of Lake Brienz and Lake Thun, the Reuss River downstream of Lake Lucerne and the Linthkanal downstream of Lake Walen. Although not all of Switzerland is covered by the study area, relevant parts of the Swiss (north alpine) social and environmental characteristics are represented, allowing for a generalization of the results on the applicability of surrogate models at a national scale.

2.2. Preprocessing for flood simulation database

In this section, we present the preprocessing steps done to create a database with flood simulation results, following the approach presented in Zischg et al. (2018a). For the scenarios, we use synthetic hydrographs similar to those created as in their study. Instead of a full 2D-flood model, we rely on semi-automatically generated 1D/2D coupled hydrodynamic models, being more efficient in simulating a high number of simulations. Compared to that study, we expand the impact assessment and the study region significantly to explore the applicability in a nationwide impact-based warning system.

2.2.1. Synthetic hydrographs

For the derivation and application of synthetic hydrographs used as upstream boundary conditions for the flood simulations stored in a database, we implement the method proposed by Serinaldi and Grimaldi (2011) and used in Felder et al.; Zischg et al. (2017; 2018a). For available gauging stations of the Federal Office for the Environment (FOEN 2023c), we manually extract event hydrographs containing only one peak and normalize these in terms of time (setting 0 as the start, and 1 as the end of the event) and discharge (based on the mean discharge over the event). The normalized average of time to peak and normalized

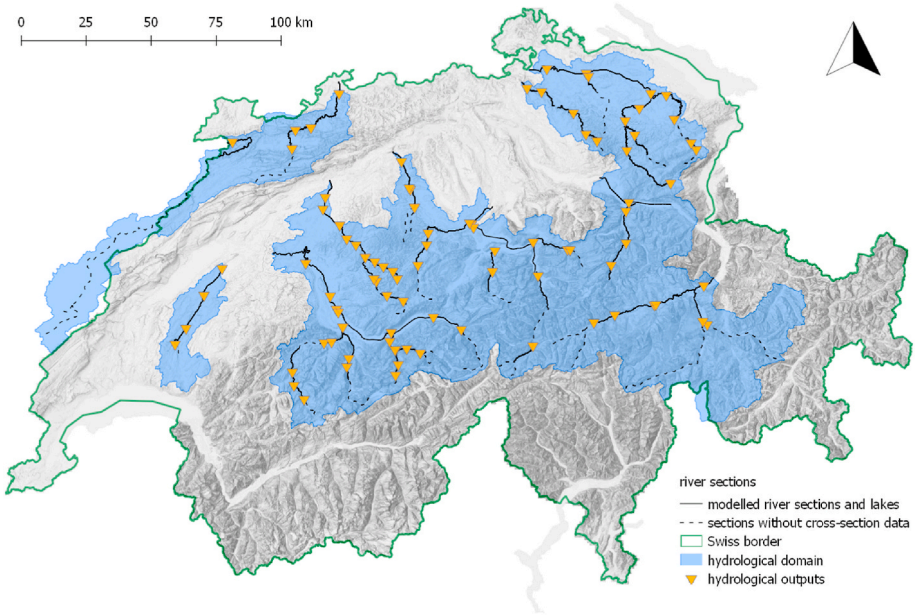

Fig. 1. Study area. The blue shaded area indicates the catchment considered in the hydrological model. The lines indicate river sections and lakes used for the hydraulic modelling/impact assessment. Triangles refer to interfaces of hydrological and hydraulic models.

average peak discharges of all events at one station are used to fit a two parametric gamma distribution function representing the typical hydrograph shape of the corresponding river or river section (Nadarajah 2007; Rai et al., 2009). The same event hydrographs extracted are also used to build a linear regression model describing the peak-volume ratio. After the fitted gamma distribution is rescaled to represent a target peak, this regression model is used to further adapt the flood volume of the rescaled hydrograph. The synthetic hydrographs are estimated for every river section individually (locations are indicated by triangles in Fig. 1) and mimic as such the typical time to peak, peak discharge relative to mean discharge and flood volume. For river sections without gauging stations, synthetic hydrographs derived by stations with similar catchment characteristics (catchment size, specific discharge) are used.

The lower limit of the range of peaks considered for the surrogate model is defined based on the threshold to warning level 3 of 5 given by the FOEN for the main part of their gauging stations (FOEN 2023a). This warning level indicates that local overtopping of river dikes is possible, the threshold is in accordance with roughly a 10- to 30-year flood, adapted based on knowledge of weak spots below this statistical value. The upper limit of the range of peaks is defined according to the highest discharge/lake level estimated by a hydrological model fed with 157 extreme weather scenarios (further details will follow in section 2.4.1 and 2.4.2) and the extreme value statistics given by the FOEN for every gauging station (FOEN 2023c). We simulate lake floodings in 10 cm steps. For rivers, the steps of discharge are set based on the lower limits of the ranges. The flood library consist of between 10 and 30 flood simulations per river section.

2.2.2. *Hydrodynamic simulations*

This study focus on the rivers of national interest in Northern Switzerland, where river cross-section measurements are taken about every 10 years by the Federal Office for the Environment (FOEN 2023b). For the hydraulic simulations, the software BASEMENT (Vetsch et al., 2018) is used. This model provides the functionality to couple 1D and 2D flood models. The cross-section measurements from the FOEN serves as data base for the 1D model, for the 2D model, we derive the topography from high resolution digital terrain models provided by either cantons (Canton de Vaud, 2004; Kanton Aargau, 2014; Kanton Kanton Luzern, 2012; Kanton Solothurn, 2014; Kanton Zug, 2013; Kanton Zürich, 2014; KAWA, 2014), the Federal Office of Topography (swisstopo 2013) or the Regierungspräsidium Freiburg/FOEN (RPF 2015). The 2D model computes the water fluxes in the floodplains based on a triangulated irregular mesh with a configured maximum area of 200 m^2 built with the meshing module BASEmesh (available as plugin for the software QGIS) integrated in BASEMENT. On average, the element size is roughly 130 m^2. To ensure that dikes and hydraulically relevant structures are considered in the 2D flood model, we digitize "breaklines" along these structures manually with the help of a hillshade generated with the high-resolution DEMs. Besides the breaklines, we manually digitize the 2D-perimeter, the 1D-2D coupling interface of the computational grid as lines as well as "flowlines" defining the river sections. This data is stored on a PostgreSQL database with a PostGIS extension also containing the cross-section data (as points and lines). With this data, a major part of the model generation can be automatized: The flowlines serve as basis to select the cross-section data needed and contains tabular information about model parameters like the friction coefficient for a specific river section. The selected cross-sections are transformed into the machine-readable 1D-model file format (BMG). An initial run to provide wet initial conditions in the 1D-model of the coupled model is automatically executed and processed. The 2D-mesh creation occurs independent of the preparation of models for single regions. Here, floodplains are meshed by discretizing all intersecting breaklines, elevation information is attributed to the mesh-nodes. After automatically meshing each floodplain, we transformed the data into the file format for the 2D-model (2DM). The 1D-2D model interfaces are stored as lines in the database, containing additional information about the model region it belongs to and whether the dike crest elevation of the cross-section data or the elevation from the DEM should be considered in the model. In case of rather small structures like walls not detected by the elevation model, it is beneficial to use the dike elevation measured and marked in the cross-section data. The model expects a list with edges defined by two node-ids whose elevation is then compared to the (linearly interpolated) water surface elevation calculated for the closest cross-section (Euclidean distance) of the 1D-model. Within a batch-process initiating the model runs, a python script updates the machine-readable BASEMENT command files (BMC) concerning simulation runtime, taken from the specific preprocessed synthetic hydrograph. A timestamp in each manually derived data is used to check for necessary updates of the simulation models. Whereas lateral 1D-2D

couplings can be derived automatically, the coupling of 1D river sections, for example to consider bifurcations/junctions, must be parametrized manually. After defining 1D-1D couplings for such cases once, the according snippets defining these couplings are stored and can be accessed again in case of an update. This guarantees consistency in the implementation of manually edited parts in the automatic setup of the command file. Due to the modular functionality of the preprocessing, updates or extensions can easily be implemented.

We calibrate the 1D hydraulic model based on stage-discharge relationships given by FOEN (2023c), optimizing the friction coefficient to fit the bankfull stage-discharge relation. Additionally, we adapt the friction coefficients in flood models where existing case studies and technical reports are available and discharge capacities are known. A major difference exists for sections where bridges are limiting the discharge capacity, as they are not yet included in our models. We assume dam stability for all our simulation scenarios, meaning that there are no dam breaches considered. A validation of the 2D flood model with the major flood events in 2005 and 2007 is not possible, because flood protection measures as river widenings or levee heightening have been implemented after these events. This makes current cross-section data inappropriate for a validation with suitable past events on regional/national scale. The study Zischg et al. (2018b) serves as a comparison, in which a similar model setup was used.

The computation as a single hydraulic model for Switzerland is currently not feasible. Therefore, regions preferably drained only by a river cross-section and not the floodplain are spatially defined. Hence, flood pathways in the floodplains are not interrupted by the model boundary. Where junctions of large or multiple tributary streams substantially increase the hydrological catchment area, river sections are divided to consider additional discharge downstream of the junction, as there is no further hydrological input other than at the upstream boundary.

2.2.3. Impact modelling

The selection of the impact variables is dependent on the targeted user or user group of IBW and IF systems. Here, we address the needs of three potential target group profiles. We want to stress that the definition of target users, their demands and their roles is not in the focus of this study. Nevertheless, to exemplify the validity of the proposed warning system, we define simplified profiles whose requirements were revealed based on a close collaboration and exchange with several stakeholder groups in Switzerland over the last years (Zischg 2023).

The first and main user group are intervention forces that manage the continuity of social life during flood events. These are disaster risk reduction and civil protection agencies like fire brigades, police or health care providers acting on both a strategic (e.g., resource management) and local emergency level (e.g., evacuations). These groups require information about flooded areas, the number of affected people, the affected infrastructure, i.e., houses, workplaces, hospitals, schools, and nursery homes. In addition, this user group requires a classification and cartographic illustration of the flood hazards, i.e., they must be informed about the locations of flooded areas that are not accessible anymore and that are critical in terms of risks for life.

The second target user group for which we test the applicability of impact forecasts are insurance companies for buildings. In 19 cantons in Switzerland, insuring of buildings against natural hazards is mandatory and regulated by public insurance companies. The insurance companies are mostly active in the aftermath of an event to make damage estimations to provide financial support. However, insurance companies can warn their customers based on their home locations before the onset of the event and must set up the claim management system within reasonable time after the event. This requires knowing the location of affected customers. With an impact forecast that provides information on flooded houses and flood damages to houses, they can prepare for managing the event by reserving organizational and financial resources. This target group thus needs information on the number of flooded houses and estimates of flood damage in monetary units from an IBW or IF system.

Lastly, we adopt the perspective of a warning service that operates a location-based alert system with the general public as target user group. These private persons ideally use the warnings to avoid dangerous areas and to reduce damage to their building and household content.

We will use these target user profiles to discuss our results in section 4. To provide the required information for the three target groups we selected the following impact variables:

- The flooded area (water depth and hazard class),
- the number and locations of flooded buildings,
- the number and locations of residents of flooded buildings,
- the number and locations of flooded workplaces,
- the number and locations of schools,
- the number and locations of hospitals,
- the number and locations of nursery homes,
- and the estimated monetary damage to flooded buildings.

Exposed objects are defined as objects that intersect computational mesh elements having been wet for at least one timestep during the simulation. We further attribute the maximum flow depth out of all intersecting elements to the exposed object as proposed by Bermúdez and Zischg (2018). The estimation of damage is done with a regionally calibrated vulnerability function based on Swiss insurance data (Zischg et al., 2021).

We classify the flooded areas into hazard classes (Table 1 and Fig. 2) following Pregnolato et al. (2017), Arrighi et al. (2019) and Costabile et al. (2021). The classification is based on the vulnerability of key elements at risk and indicates hazards for people inside and outside of

Table 1
Classification of hazard classes, where h denotes flood depth and v flow velocity.

Class	Description	Constraints
0	Not exposed to floods	$h < 0.01$ m
1	Flooded but safe for pedestrians and vehicles	$h < 0.3$ m AND $v < 2.0$ m/s AND $h*v < 0.3$ m^2/s
2	No access for vehicles	$h > 0.3$ m OR $h*v >= 0.3$ m^2/s
3	Pedestrians and/or vehicles highly vulnerable	$h > 0.5$ m OR $v > 2.0$ m/s OR $h*v >= 0.6$ m^2/s
4	Considerable damage to buildings expected	$h > 1.5$ m

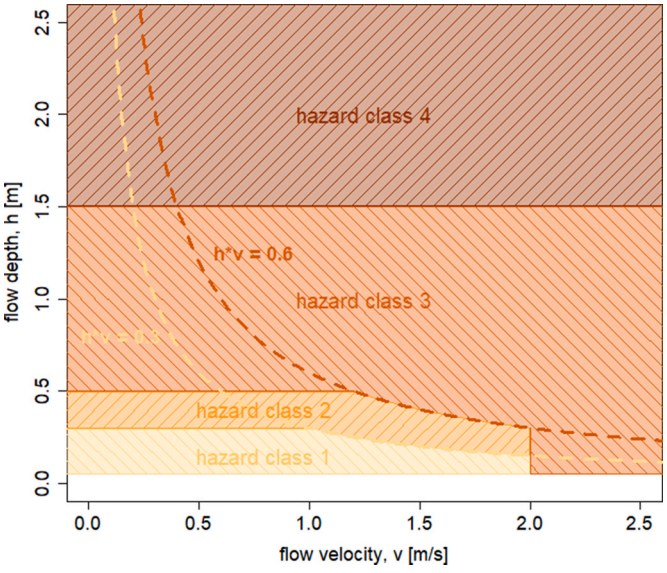

Fig. 2. Schematic of hazard classification as defined in Table 1.

buildings and for cars. The maximum hazard classes from each pre-calculated scenario are stored in the database specific for each element, as the hydraulic model outputs the required variables.

2.3. Implementation in early warning systems

The approach as one element of the modelling chain can be coupled to any hydrometeorological forecast. A transient modelling approach with the same spatiotemporal resolution as used to precalculate flood scenarios for the database is not suitable for early warnings, as the simulation time would exceed the lead time of the hydrometeorological forecast.

After the preprocessing described in the previous section, hazard information and the corresponding peak discharge is stored in a database for every mesh element, together with spatial information of exposure data (in our case a PostgreSQL database with a PostGIS extension). To improve performance, we preprocess a matching table of elements from the computational mesh and exposure data. With any given hydrological forecast, the corresponding peak discharges from the predicted hydrographs serve as basis to select the scenario calculated with the peak closest to the *predicted* peak. Technically, this corresponds to a *k*-nearest neighbor analysis with $k=1$ based on Euclidean distance. After that, the matching table allows to join impact data to the flood surrogate model. This can then be visualized cartographically along with a quantitative summary of the impacts at a desired level of aggregation, even for the entire study area. This can all be achieved in just a matter of minutes. The high performance also allows, e. g., to consider multiple members of an ensemble or to implement a routine considering multiple hydrometeorological forecasts to account for uncertainties. E.g. by setting $k=2$, the precalculated scenarios with the next higher and lower peak discharges are considered.

In certain cases, a clear separation of rivers is not possible but still necessary, as it is for example the case near junctions, where floods from two joining rivers can affect the same floodplains. The setup of the flood surrogate model for this case is summarized schematically in Fig. 3, showing that we define a subdomain as one river section with the corresponding floodplain. Here, the surrogate model combines the simulations of the three subdomains (two upstream, one downstream). Every subdomain requires a hydrograph from the hydrological model to select the scenario based on the correct peak discharge. Preparing thorough simulations for a surrogate model at junctions would require simulating multiple combinations of peak discharges in the two upstream rivers. If for example each of the three considered river sections consists of about 20 precalculated scenarios, this would end up in 400 ($=20 \times 20$) instead of 60 simulations to consider all possible combinations of the two upstream subdomains, assuming that there is no or just minor additional discharge from any other source. To compare a surrogate with a transient model in such a region, the flood predictions of all subdomains (A, B and C in Fig. 3) in a model region are merged. This means that multiple subdomains might be the source for flooded areas when their floodplains can't be separated topologically. In such cases, the highest magnitude is retained. In a model region with only one river section (= only one subdomain), the procedure is the same, but without the need to merge subdomains. Therefore, impact could directly be derived from "flood magnitude – flood loss" relationships as described in Zischg et al. (2018a). In terms of performance, there is no significant gain of time when doing so, as the join via matching table is already very performant and necessary anyway to provide flood maps. We will present and discuss our results based on the model regions.

2.4. Evaluation of the surrogate models

The simplified surrogate model is tested for replacing a time-consuming transient simulation model. This requires measuring the loss of information due to the approximation. For the evaluation of the library-based surrogate flood model, a set of extreme precipitation events is created from hindcast archives leading to floods over a large scale of hydrological Switzerland. After extracting these events from hindcast archives, transient simulations with the hydrological model DECIPHeR and the same hydrodynamic model used for preparing the flood simulation library are applied. For both modeling approaches, the flood impacts are calculated. The results serve as benchmark to measure the accuracy and computational performance of the surrogate flood model to represent the transient simulation.

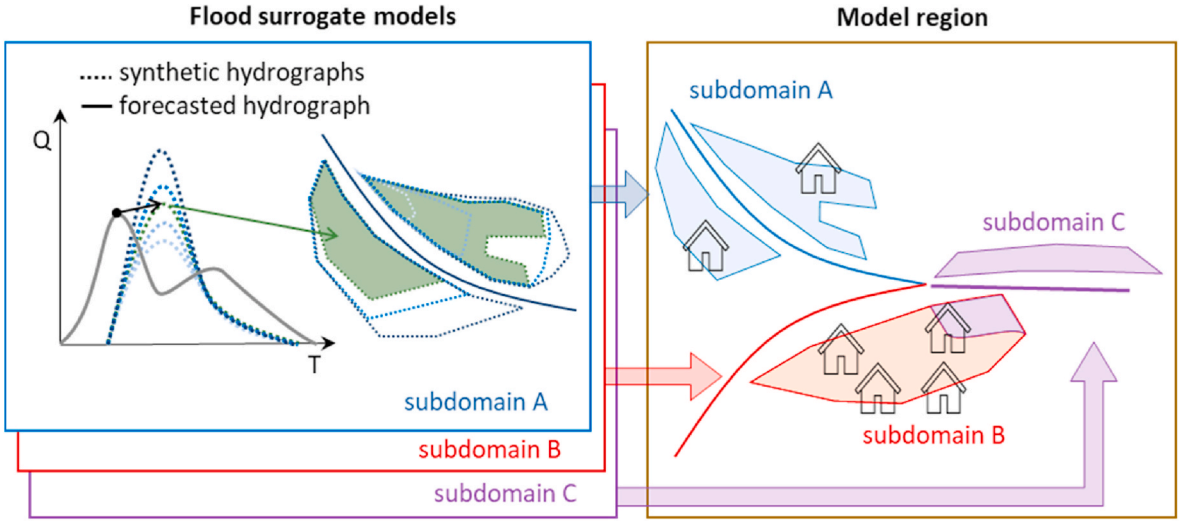

Fig. 3. Schematic illustration of the functionality of the flood surrogate model during a forecast, in this illustrated example, consisting of three subdomains A, B and C. Together, the subdomains are defined as one model region (coupled in transient model). Hazard and exposure data is stored on the same database. The spatial relation of every mesh element to the building footprint is preprocessed and stored as a matching table. Flow depth, velocity and the hazard class are stored for every element in an hourly resolution, specifically for each subdomain and each precalculated scenario (based on synthetic hydrographs, dotted lines in discharge (Q) - time (T) diagram). In case of a forecast (straight grey line in Q-T diagram), the scenario with nearest peak is selected (dotted green line and corresponding green area) and combined with exposure information via matching table. This serves as basis to calculate impact. In case of overlapping flood zones of subdomains (here: B + C), the maximum flow depth for each element is used (here: C, illustrated by the filled color).

2.4.1. Meteorology

To validate the surrogate modelling approach with precipitation events of high return periods that are hitherto not observed, we apply the reforecast pooling method (UNprecendented Simulated Extreme ENsemble, UNSEEN) as presented in Thompson et al. (2017) and Kelder et al. (2020), using the hindcast archive of the European Centre for Medium-Range Weather Forecasts (ECMWF) extended-range forecasts ENSext as well as the seasonal forecasts SEAS5 (Johnson et al., 2019; Stockdale 2021).

To arrive at the spatial and temporal scale of the hydrological model, we:

1. Downscale the hindcast data from a regular 0.4° grid to a spatial resolution of 2 km using quantile mapping (Ivanov and Kotlarski 2017; NCCS 2018),
2. and linearly disaggregate the resulting fields from 6-hourly to 1-hourly timesteps.

As reference data to downscale precipitation we use a merged data set consisting of CombiPrecip (Sideris et al., 2014) and Cosmo Rea2 spanning the period 2005–2017. For temperature and evapotranspiration, we use Cosmo Rea6 for the same period. The Cosmo Rea reanalyses (Wahl et al., 2017) include several products, amongst them Cosmo Rea2 and Cosmo Rea6. Both have a temporal resolution of 1 h but differ in the spatial resolution (approximately 2 km vs. 6 km) and period (Cosmo Rea 2 2007–2013 vs. Cosmo Rea6 1995–2017, see also Meteorological Institute of the United Nations (2015)).

To select individual spatially distinct precipitation events with a certain probability of occurrence, we pool all precipitation events in the hindcast data: First, we compute the 6 hourly time series of running accumulation of area precipitation over the whole hydrological domain of Switzerland, defining this as the feature describing the precipitation events. The time series is then declustered in time such that the precipitation events (and the corresponding accumulation time windows) do not overlap. In order to estimate a return period for the events, we compile the discontinuous hindcasts into pseudo-years, pool both ENSext and SEAS5 together, and fit a GEV distribution (e.g. Coles 2001) on the resulting yearly blockmaxima.

Finally, we select all events for accumulation periods of 3 and 5 days, which are usually leading to larger discharge peaks, and are the typical durations relevant for the generation of floods in small to mesoscale catchments or catchments with lakes, resulting in a total of 157 events. Each selected event contains nine 1-hourly extra time steps at its start and 10 1-hourly time steps at its end. Note that precipitation in the extra time steps is not considered for the extraction of the events based on the return periods.

2.4.2. Hydrological modelling

The hydrological model DECIPHeR is used to infer river discharge from precipitation, temperature and potential evapotranspiration information for the selected extreme weather events (Coxon et al., 2019). To meet the requirements of the complex mountain topography in Switzerland, modules for modelling snow and ice melt need to be added to the original code, similarly to Shannon et al. (2023). We implement a classical temperature-index (TI) melt model, which is solely based on air temperature and linearly relates melt rates to air temperature by a melt factor differing for snow and ice surfaces (Gabbi et al., 2014), where the threshold temperature distinguishing between melt and no melt accounts for the fact that melt is controlled by the energy budget at the surface and can also occur at air temperatures below and above the melting point of snow and ice (Gabbi et al., 2014; Kuhn 1987). Additionally, routing and storage modules such as regulated lakes and reservoirs are introduced into the hydrological model.

We perform a split-sample calibration-validation for the hydrological model using data between 2005 and 2007 for the calibration and 2008 and 2010 for the validation (see goodness of fit measures in Appendix B). In 2005 and 2007, two of the largest floods impacting a vast area of the Northern Swiss Alps took place, and as such represent a good calibration ground, being the main aim of the tool the simulation of floods. The period between 2008 and 2010 was chosen considering the inhomogeneity in CombiPrecip, for which in 2011, all three radars it is based on were replaced and the period from 2012 on seems to have a stronger tendency to underestimate precipitation, in particular in the first three years (Panziera et al., 2018). The "dry" biases are present already in the years used for calibration and validation, mainly in Autumn and Winter, when there are less convective storms and the visibility of the radars becomes a major limiting factor. The largest uncertainties are expected close to the national boundaries, where the number of precipitation gauging stations at the ground drops, and in the Eastern part of Switzerland, as well as the Rhone valley (Betschart, 2012).

The initial conditions for the hydrological simulations are created using observations from the CombiPrecip dataset of MeteoSwiss (Sideris et al., 2014; MeteoSwiss 2017) with a two years model spin-up. All selected 157 extreme weather scenarios from the hindcast archive are inserted into the year 2010 (a year with average conditions) of CombiPrecip, considering the original season of the hindcast data: winter events (December to February) were inserted on 1 February 2010, spring events (March to May) on 5 April, summer events (June to August) on 15 July and autumn events on 1 November. After inserting the events, the hydrological model is run continuously until the end of the year, this way we ensure that delayed peaks of discharge or maximum levels of lakes reached after the duration of the extracted time window of the weather event are present in the hydrographs.

Finally, out of the 157 extreme precipitation events, nine are selected based on the location of the highest precipitation accumulations and on the temporal evolution of the precipitation events (events with one or two precipitation peaks during three or five days). We consider scenarios with precipitation maxima over western, central as well as eastern Northern Switzerland and scenarios with hotspots over alpine, prealpine and plateau regions. The scenarios cover different return periods, and we choose scenarios that lead to peak discharges exceeding the ones measured during any flood event along the river network (see Fig. 4).

Note the naming of the scenarios (e. g. 03d-1000y_05) used in subsequent sections: The first part of the scenario name (05d, 03d) indicates the duration in days, the second part (100y, 300y, 1000y) the return period of the precipitation sum averaged over the hydrological domain of Switzerland, the last part corresponds to the event number (no physical meaning).

2.4.3. Transient flood simulations and impact assessment

The simulations in both model setups (transient model/surrogate model) are based on the same irregular mesh with the same elevation information. Differences can be found in multi-domain regions, e. g. with junctions: the subdomains in the transient flood model are directly coupled (1D and 2D), an upstream boundary condition is only defined for the two upstream subdomains, whereas the discharge for the downstream subdomain is calculated hydraulically. There is no difference between the transient model and the surrogate model approach concerning impact assessment.

2.4.4. Validation with metrics

To analyze the potential of implementing the flood surrogate models into IBWs and IFs, we assume the nine weather scenarios together with hydrological, hydrodynamic and impact calculations derived with the transient model to be the observation and thus the benchmark against which the surrogate models are compared. This means that the hydrological output is used at the same time also as input to select the surrogates, being this the forecast the surrogate model has to operate with. Thus, we implicitly neglect the uncertainty present in the modeling steps before the application of the flood surrogate model, and only bring into focus the uncertainty in the latter.

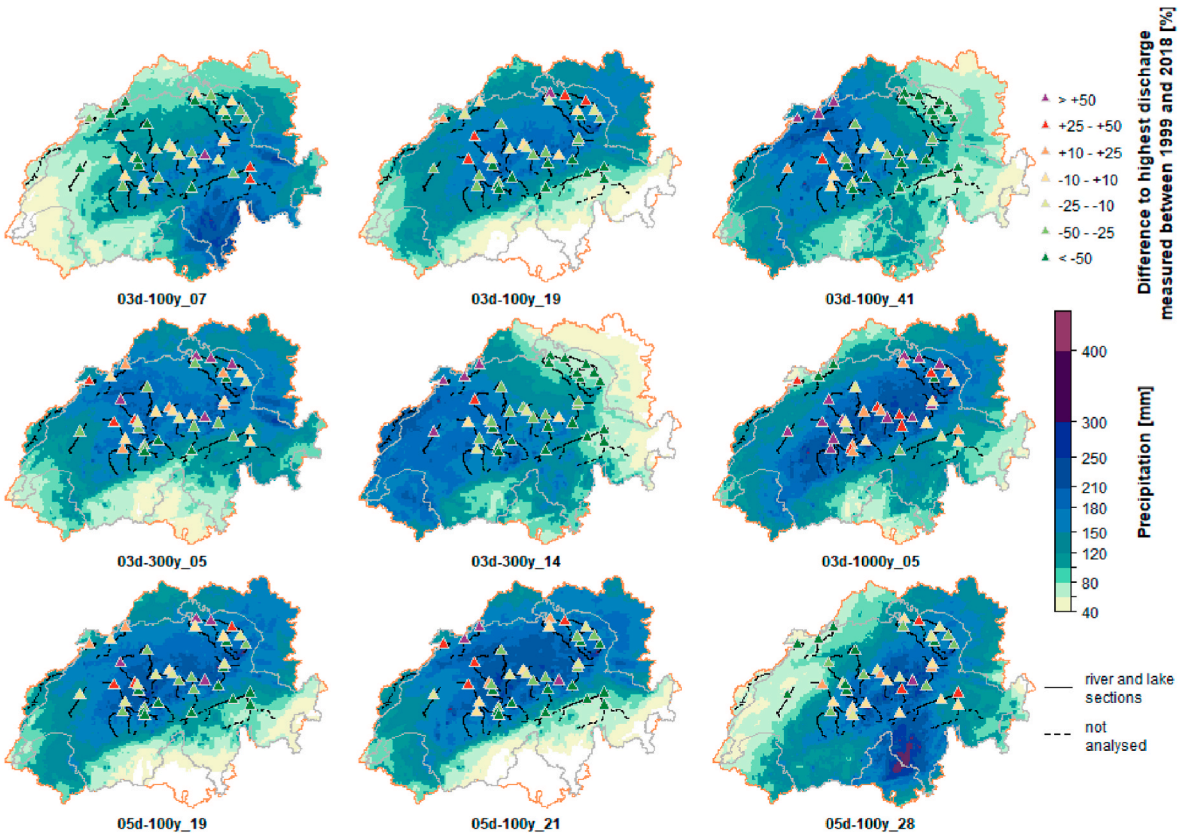

Fig. 4. Precipitation sums extracted with UNSEEN method (mm, color shading), together with deviation (%) of the modelled discharge from the highest discharge measured at gauging stations within the study area between 1999 and 2018. The orange outline defines the Swiss hydrological domain, the Swiss boundary is plotted in grey, scenario names are indicated below.

For every river section, we extract the peak discharge from the hydrological model and compare the impact of the hindcast event with the outputs of the closest precomputed simulation.

To objectively assess the quality of the surrogate model, we use validation metrics from Bennett et al. (2013), e.g., the Critical Success Index (*CSI*), also used as Model Fit (*F*) in Zischg et al. (2018b) when applied for exposed buildings or as Flood Area Index (*FAI*) in Falter et al. (2013), where flooded area is of interest. In this study, we will use the term "*Model Fit*" independently, e.g., for flood area, flood volume, buildings, people, or workplaces:

$$Model\ Fit\ (F) = CSI = FAI = \frac{S1T1}{S1T1 + S1T0 + S0T1} \tag{1}$$

where *S1T1* denotes the agreement (hits) between transient model approach (*T*) and the surrogates (*S*), *S1T0* are, for example, areas defined as wet by the surrogate but dry by the transient model (false alarms) and *S0T1* vice versa (misses).

Additionally, we use the *BIAS* score as indication whether the surrogate models over- or underestimate hazard and impact compared to the transient model. The *BIAS* score is calculated as follows:

$$BIAS = \frac{S1T1 + S1T0}{S1T1 + S0T1} \tag{2}$$

A *BIAS* score higher than 1 will therefore indicate an overestimation by the surrogate, whereas values below 1 indicate an underestimation.

3. Results

The results of our analysis are structured as follows. First, we compare all synthetic hydrographs from the surrogate models with the hydrographs from the transient simulations (section 3.1). After that, we compare the results from the flood simulation (section 3.2) followed by an analysis of the impact (section 3.3). We follow Zischg et al. (2018b) to define the goodness of fit of the surrogate models matching hazard and impact modelled with the transient approach. Finally, we also bring in the temporal aspect related to the propagation of the flood (section 3.4). The results rely on transient simulations done for 78 model regions. To cover all subdomains in these model regions, 1881 flood scenarios in 101 subdomains (= single river sections and its floodplain) had to be precalculated for the flood scenario database used by the surrogate model. With using two cores per simulation, 78 of 101 subdomains simulate with a real-time speed up (*rts*) of more or equal 10, 14 subdomains with an average *rts* between 3 and 10, eight subdomains with a *rts* between 1 and 3 and only one subdomain (lake Lucerne) with a *rts* below 1 (0.9). The simulations are executable via batch-process and are run in parallel computing on two 10-cores (20 threads) Intel Xeon E5-2660 v3 (2.6 GHz) processor units.

3.1. Hydrograph matching

The combination of 78 model regions with nine extreme weather scenarios (=702 transient model runs) results in a total of 310 floods. Fig. 5 shows the relative difference of the peaks and volumes of the selected synthetic hydrographs and the hydrographs generated in the transient simulation model for all river reaches, excluding lakes and river sections with lake levels as upstream boundary. Here, the difference from the full model to the surrogate can maximally be 5 cm, as lake levels were simulated in 10 cm steps. For most river sections, the difference in peak discharge from synthetic to transient model hydrographs is about ± 5%. The discharge volume is systematically underestimated by synthetic hydrographs. Note that for the volume only timesteps above the minimum calculated peak in the flood library were accounted.

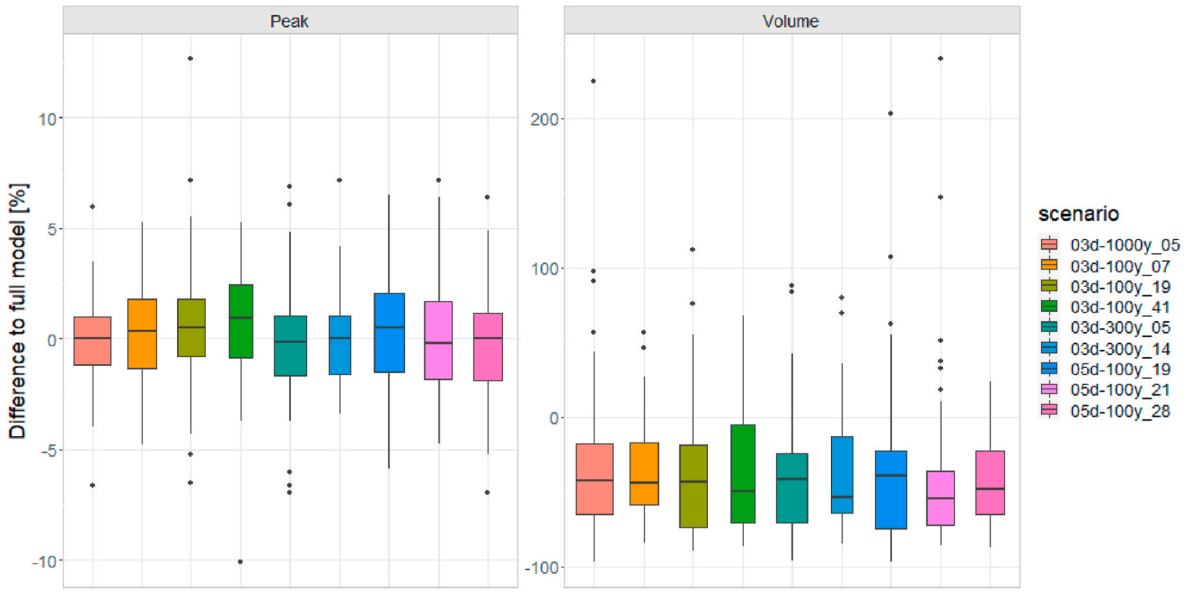

Fig. 5. Relative differences in hydrographs for 78 model sections in terms of peak discharge and discharge volume above the smallest simulated peak considered in the libraries. Lake hydrographs are excluded. For the naming of the scenarios, see the last paragraph in section 2.4.2.

According to FOEN (2023a), this is the threshold where first river or lake floodings might occur.

Fig. 6 illustrates one major source of underestimation: Whereas the (main) peak of the hydrograph after two days is well represented by the synthetic hydrograph, the flood relevant volume before two days is not covered. Flood volume driven differences between surrogate and transient model can therefore be expected mostly in floodplains where discharge capacity was exceeded already in the first phase of this event.

3.2. Prediction of flood hazard variables

In this section, we focus on the comparison in terms of hazard variables like flooded area, flow depth and flood volume in the floodplains of the model regions. To derive "overall" metrics, we aggregate *S1T0*, *S1T1* and *S0T1* over all model regions and scenarios, meaning that one region is considered multiple times when floods occurred in more than one scenario. We remind the reader that one region can consist of multiple river or lake sections (e.g., at river junctions), when a clear separation of floodplains was not possible (described in section 2.2.2). The overall *Model Fit* in terms of flooded areas (*FAI*) for the entire river network is 0.84, the *BIAS* score of 1.014 indicates that over- and underestimation are balanced over the entire study area. As the overall metrics are dominated by model regions with extensive floods, Fig. 7 shows the distributions of calculated *Model Fits* and *BIAS*' for model regions grouped in 10%-quantile ranges of the flooded area in the transient simulation. The area of the river channel (1D model) was not considered to calculate the *Model Fits*.

Although the distributions among the quantiles are not significantly different from each other, there are certain tendencies that can be observed. On the one hand, the more pronounced low *Model Fits* in the first two quantile ranges (1: 0–10%, 2: 10–20%) and their higher variability in the *BIAS*' indicate higher uncertainties in regions where the flooded area is small. On the other hand, there is a slight negative but non-significant tendency in accuracy for the highest quantile range, with a median lower than 0.9 and an underestimation of the flooded area. Although a major part of the *Model Fits* being calculated per scenario and

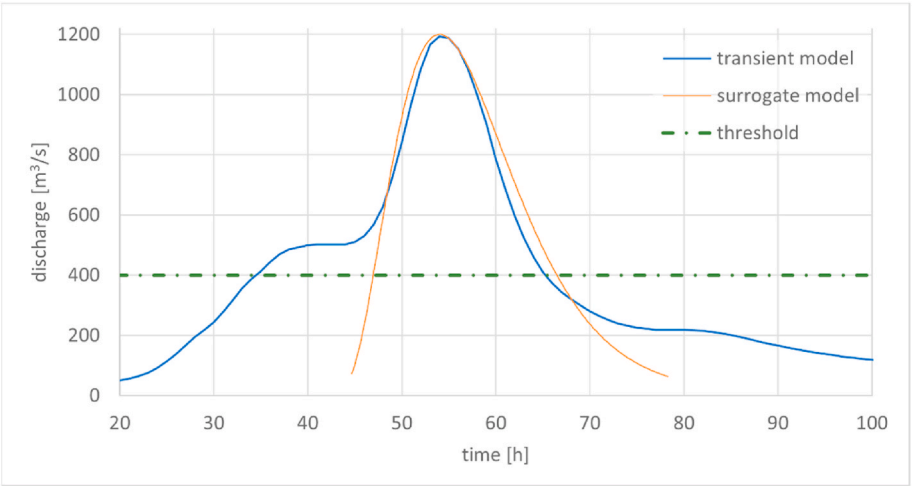

Fig. 6. Hydrographs of Emme river near Burgdorf, simulated by the hydrological model (blue, scenario 03d-1000y_05) and derived synthetically (see section 2.4.2) for the matching surrogate (orange), fitted by peak discharges. The lowest peak discharge calculated for the Emme river near Burgdorf is 400 m^3/s (=threshold). Even though the volume above this threshold is about 25% higher in the transient model due to the first phase of the event, the visual impression of the synthetic peak fitting the "main peak" of the full hydrograph is good.

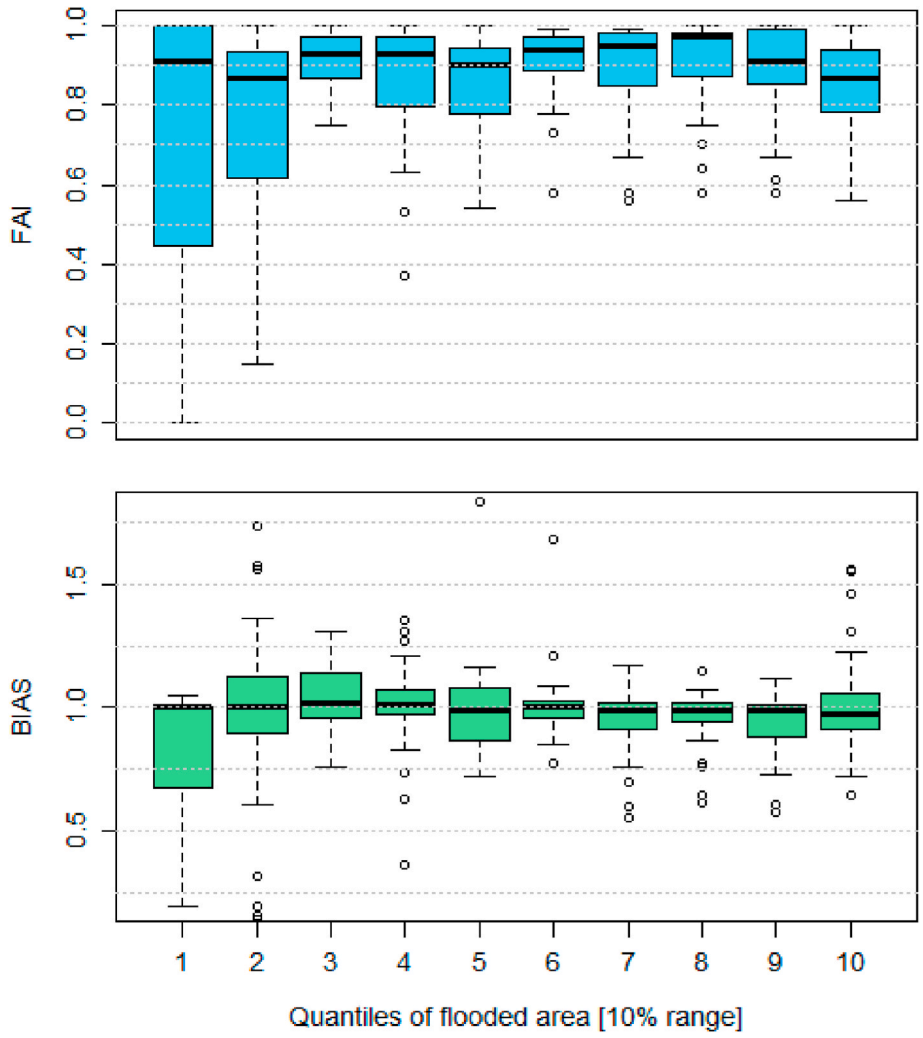

Fig. 7. *Flood Area Index* (top) and *BIAS* (bottom), the values used for the boxplots represent indices specific for a combination of model region and scenario (totally 310 floods). The boxplots show the distribution of the indices for each quantile range of flooded area. Depending on the flood area specific for scenarios, a model region can be represented in different quantiles. The 10%-quantile ranges contain regions with following flooded areas (in 10k m^2 = hectares): Q1: 0–0.3; Q2: 0.3–1.2; Q3: 1.2–3.1; Q4: 3.1–6.4; Q5: 6.4–16; Q6: 16–33; Q7: 33–57; Q8: 57–87; Q9: 87–241; Q10: 241–2972.

region is higher than calculated overall (0.84), it's mainly the upper two 10%-quantiles that influence this value sharing more than 84% of the total flooded area by the flood model. The regions with flooded areas in the lower five quantiles only share 2% of the total flooded area. Besides flood extent, the intensity of the flood influences the impact. Therefore, we compared calculated flow depths of the transient with the surrogate model based on 2.6 million mesh elements. Table 2 shows the quantiles of the flow depth differences calculated by the transient model to the matching simulations of the surrogate model. 80% of all elements show differences less than 20 cm (*overall, Q10 – Q90)*, 5% of the elements show overestimation of more than 46 cm, 5% underestimate flow depth by at least 35 cm. Considering all elements (*overall*), the zero median together with similar positive and negative values for the quantile ranges (e. g. when comparing Q10 with Q90) indicates a low *BIAS*.

Replacing flooded area with maximum flooded volume in the floodplain (area multiplied with flow depth in equation (1)) results in slightly but significantly lower overall *Model Fits* (see Appendix A). This can be considered as expected, as the influence of flow depth adds another level of complexity and uncertainty, although the differences in flow depths are not high for most of the elements. The overall *Model Fit* based on flood volume is 0.81, the *BIAS* score 1.000. Besides a generally lower *Model Fit*, there are similar findings as for the flood area.

3.3. Prediction of impact

Next, we evaluate the quality of the flood impact estimation by the flood surrogate model. First, we compare exposure of hospitals, schools and nursery homes. Then, we evaluate the simulated hazard classes (as

Table 2
Quantiles of flow depth differences in meters (transient model – surrogate). Negative values indicate overestimation of flow depth by the surrogates, positive values an underestimation. *S1T1* = wet in surrogate and transient model, *S1T0* = wet in surrogate but dry in transient model, *S0T1* vice versa.

	Min	Q5	Q10	Q25	Q50	Q75	Q90	Q95	Max
S0T1	0.01	0.01	0.01	0.03	0.1	0.28	0.71	1.12	4.12
S1T0	−4.67	−1.06	−0.83	−0.52	−0.25	−0.08	−0.02	−0.01	−0.01
S1T1	−3.09	−0.29	−0.08	−0.01	0	0.04	0.15	0.3	2.79
Overall	−4.67	−0.46	−0.2	−0.03	0	0.04	0.17	0.35	4.12

defined in section 2.2.3) of the surrogate models by comparing them with the hazard classes simulated by the transient model: We compare the hazard classification of area, buildings, persons and workplaces (Fig. 8). Finally, we compare the flood damage estimation from the transient model and the surrogate approach.

Over all scenarios and regions, 20 nursery home locations are modelled as exposed 62 times in the transient model, five are missed by the surrogate models without any false alarm. In the scenarios 03d-1000y_05 and 05d_100y_28, the model region of the river Muota near Brunnen contains 5 buildings within a hospital area being exposed in both models. In terms of buildings within school areas, 372 (153 unique buildings) are modelled as exposed by the transient model, whereof 49 were modelled as dry by the surrogates (misses). 15 buildings were modelled wet by the surrogate but dry by the transient model (false alarms).

The *overall Model Fits* calculated for buildings (0.88), persons (0.89) and workplaces (0.92) are considerably higher than these for area (0.84) and volume (0.81). This indicates that roughly nine out of 10 buildings, persons or workplaces receive a warning for potential exposure to a flood from the transient as well as from the surrogate model. When additionally penalizing wrong hazard classifications, the *Model Fits* are reduced to 0.74 for area, 0.78 for buildings, 0.8 for persons and 0.83 for workplaces. This means that e.g., eight out of 10 persons would receive the same warning of the severity of impact (one person out of 10 would be similarly informed about exposure, but different about the consequences). Note that the Model Fits for the hazard classes cannot exceed the "general" *Model Fits*. Fig. 8 gives further details on the quality of hazard classification by the surrogate model.

We see that the second hazard class, showing areas/roads that are no longer passable by vehicles, is underrepresented compared to hazard classes 1 and 3. In this hazard class, only 69% of the area modelled by the transient model is also modelled as hazard class 2 by the surrogate model, what is considerably lower as found for class 1 (81%), 3 (83%) and 4 (86%). There are similar findings for buildings, workplaces, and persons. As hazard class 2 is defined for flow depths between 0.3 and 0.5 m and e.g., the *RMSE* of flow depth is 27 cm, the definition of class 2 is probably not suitable for the approach presented. Persons and workplaces have a higher relative exposure in hazard class 3 and 4 compared to area or buildings, these two classes are also better represented by the surrogates independent of the variable. Furthermore, the number of misses in exposure of buildings, persons, and workplaces (green bars) compared to the number of false alarms (colored bars at x = 0) is higher, indicating an underestimation *BIAS*. This is supported by the *BIAS*' in Appendix C, showing that mainly the exposure in scenario 03d-300y_14 is underestimated.

We propose a visualization of the impacts on a map as shown in Fig. 9. Together with a highly resolved map, information is given about accessibility of certain areas or buildings, regions where people potentially are endangered inside or outside a building and regions with potentially highly vulnerable buildings (school and hospital areas, nursery homes).

Finally, we compare damage estimates from both model set-ups. Table 3 gives an overview of the damages calculated using the transient and the surrogate model. In two scenarios, 03d-100y_41 and 03d_300y_14, the damage is underestimated by the surrogate model with −15.4% and −27.2%. On average the damage is underestimated by the surrogate approach by −7%. The section of the Emme River from Burgdorf to the junction with the Aare River contributes to this underestimation and is – same as the aggregated damage for each scenario – underestimated in most scenarios. The underestimation of damage in this region amounts to CHF -141 million (−76.1%) in scenario 03d-100y_41 and CHF -303 million (−55.3%) in scenario 03d_300y_14, explaining a major part of the total difference in damage.

As the Emme river floodplain is of major importance and systematically underestimates flood hazard and impact, we tried to assess the reasons: 1) In the first scenario mentioned above 03d-100y_41, one major retention area in the modelled region is not filled to its capacity in the surrogate model, whereas this is the case in the transient model. Therefore, even though the peak discharge is lower in the transient simulation, the outflow out of this retention area hits an industrial area with many large buildings with high values and therefore results in high damage. Something similar happens in scenario 05d-100y_21.2. In

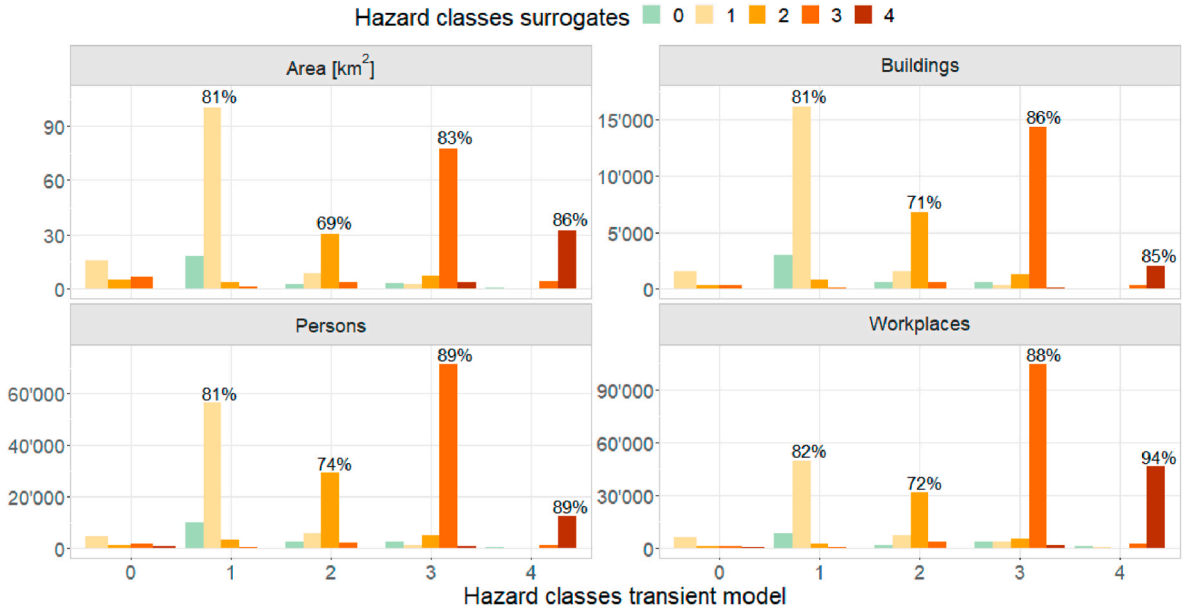

Fig. 8. Comparison of hazard classification of area (top left), number of buildings (top right), number of persons (bottom left) and number of workplaces (bottom right) by the transient model and surrogate model. The color of the bars indicates the classification given by the surrogates, the allocation at the x-axis the hazard class given by the transient model. The y-axis shows the numbers related to the title of each facet. The percentages on top of the bars indicate the fraction of the area, buildings, persons and workplaces classified by the transient model that is represented by the surrogates. Workplaces and Persons were allocated to buildings. Green bars represent the misses of the surrogates (S0T1), the bars located at the hazard class 0 of the transient model (left most category in each facet) represent false alarms (S1T0).

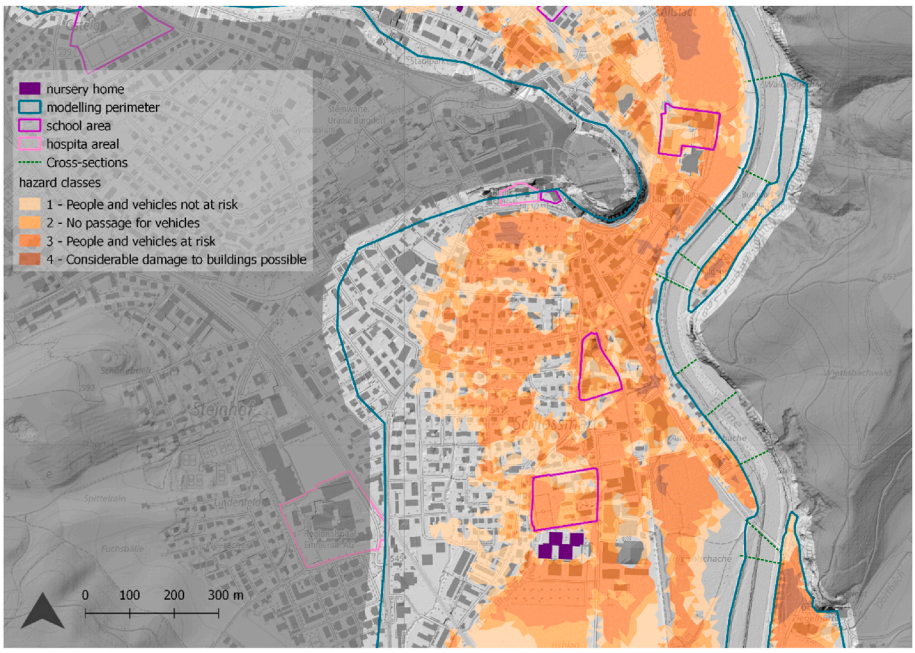

Fig. 9. Example of hazard map (from the surrogate model) of the Emme river near Burgdorf to support civil protection indicating predicted impact for people, vehicles and buildings and showing areas and buildings with vulnerable people (background swisstopo (2013; 2023)).

Table 3
Comparison of scenario specific damage estimates based on the full model and surrogate model. For the naming of the scenarios, see the last paragraph in section 2.4.2.

Scenario	Damage transient model [CHF million]	Damage surrogate model [CHF million]	Difference [CHF million]	Difference [%]
03d-1000y_05	5460.11	5161.46	−298.65	−5.5
03d-100y_07	598.19	647.07	48.88	8.2
03d-100y_19	919.78	869.95	−49.83	−5.4
03d-100y_41	890.59	753.41	−137.18	−15.4
03d-300y_05	1738.74	1582.91	−155.84	−9
03d-300y_14	1176.06	856.72	−319.35	−27.2
05d-100y_19	1188.33	1098.44	−89.89	−7.6
05d-100y_21	1393.85	1358.49	−35.36	−2.5
05d-100y_28	1590.38	1583.04	−7.35	−0.5
Overall	14956.04	13911.49	−1044.55	−7

scenario 03d-300y_14, the peak discharge of the transient model is almost in the middle between two synthetic hydrographs but matches best the one with a lower peak. However, the second-best surrogate with a higher peak discharge would lead to an overestimation of the flooded area and therefore most likely of the damage. It can also be observed in scenario 05d-100y_19, 03d_100y_19 (see Fig. 10, left) and 03d-300y_05 that the impact assessed by the transient model is in between the best surrogate with a lower and the second-best with a higher peak. 3). Similarly, the reasons for the underestimation in scenario 03d-1000y_05 (−13.6% = CHF -223.5 million) might be the missing flood volume above the river capacity before the main event (see Fig. 6) and the floodplain interactions over multiple subdomains that were modelled separately in the surrogate but together in the transient modelling approach. In general, a Mann-Whitney *U* test indicates that the *Model Fits* in regions with floodplains where floods can result from multiple rivers or lakes, and therefore interactions are possible, are significantly lower (median 0.86 compared to 0.94, no significant difference according to Kolmogorov-Smirnof test). In case of a river junction, the fitting of the scenario for the downstream river section is based on the hydrological output that is not considering peak attenuation. This effect is found in scenario 03d-1000y_05 in the model region enclosing Frauenfeld. In this region, the river Murg flows into the river Thur. The attenuation of the peak discharge in the upstream section of the Thur (from 1600 m^3/s to roughly 1300 m^3/s) is not modelled by the hydrological model and therefore also missing in the surrogate model, leading to an overestimation of the flood in the downstream section (see Fig. 10, right). This is in agreement with Farrag et al. (2022) and Viviroli et al. (2022) who state that retention/attenuation effects should be considered in the modelling chain.

The present analysis is conducted to determine the next-to closest fit ($k=2$) for the surrogate model. Out of the 310 model regions considered, 51 regions reach a superior *Model Fit* in terms of area (*FAI*). Among these regions, the increase ranges from 0.06 to 0.22 in 22 cases, and from 0.25 to 0.62 in five cases with rather low flooded areas (lower 20% of all simulations). Additionally, the transient model simulated a larger flooded area compared to both nearest neighbors from the surrogate model in 46 out of the 310 cases, while in 18 cases it was smaller. This means that in 246 cases (79.4%), the two closest fits surrounding the peak magnitude are able to estimate the range of the potential flood extend. Specifically aggregated for each scenario, the *Model Fit* can only exceptionally be improved by choosing the next-to closest fits. Compared to the loss in certain cases (up to 0.29), the potential gain (up to 0.06) is small (see Appendix D).

Fig. 11 shows the relative differences of damage estimates between the transient model and the surrogate model, where every dot represents the damage of one model region in a specific scenario. Note that only in 259 combinations out of 310 flooded model regions (over all scenarios) buildings are exposed and therefore damage estimated. We see that high

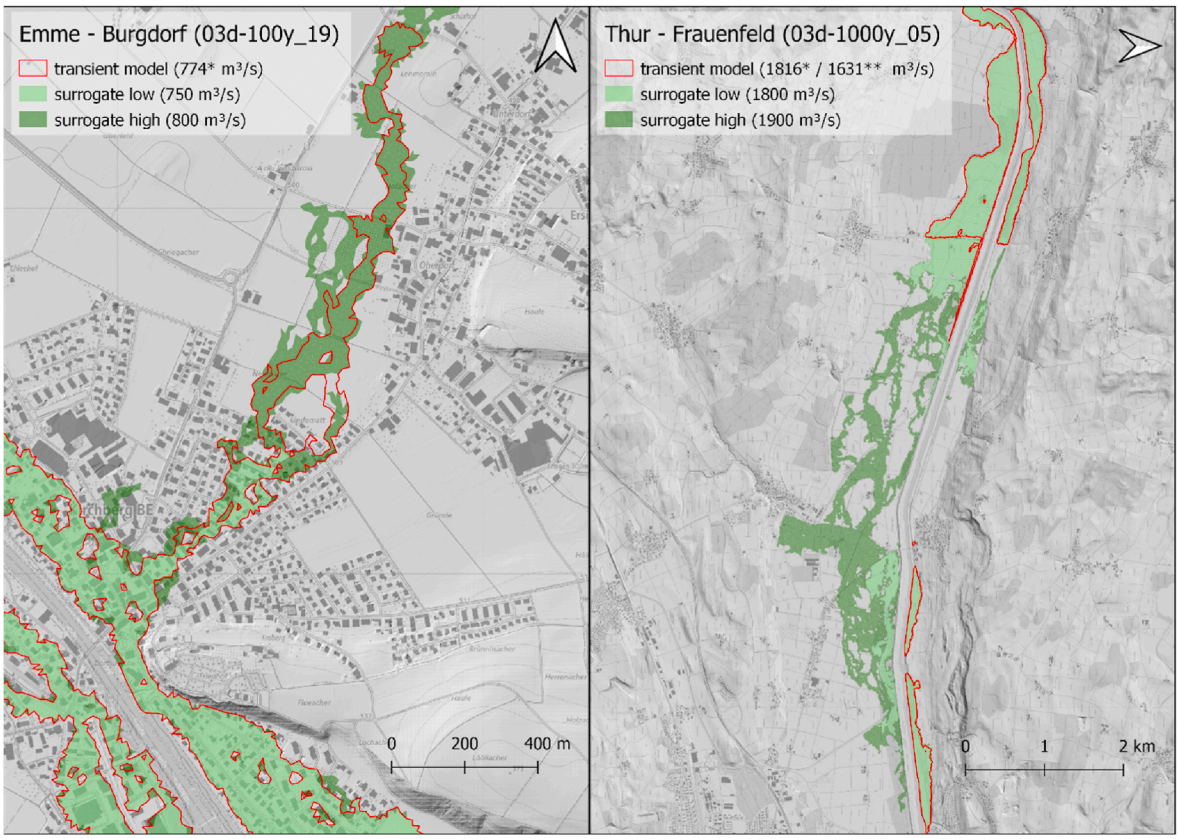

Fig. 10. Flood perimeters of the transient model simulation (red polygons) and the two nearest precalcuated scenarios according to peak discharge (light/dark green area). Left: one subdomain of Emme River near Burdgorf (N 47.05866°, E 7.61725°) showing that the surrogate with lower peak underestimates, and the surrogate with higher peak rather overestimates the transient simulation. Right: Downstream subdomain of the Thur River near Frauenfeld (N 47.55885°, E 8.90714°), showing that the surrogate with the higher and the lower peak overestimate the flood perimeter of the transient simulation, as peak attenuation in upstream subdomains and additional tributaries along the river reach of the Thur in this region is not considered. Note that the maps are drawn at different scales and the right map is rotated by 90°.

* Discharge calculated by the hydrological model and used to select surrogate

** Hydraulically calculated peak discharge in transient model (lower due to peak attenuation in the upstream subdomain).

relative differences in losses occur in regions with low absolute damage. Additionally, we see that in regions with damages above CHF 10 million, there are five cases with positive or negative differences of more than 50% (- > two cases of Emme Burgdorf mentioned above), four model regions with differences from 30 to 50%, 21 regions with differences from 10 to 30% and 68 regions with a difference below 10%.

3.4. Temporal aspects

Besides the spatial evolution during an event, the chronology of a flooding is also important. For preparing evacuation measures, for example, the time lag of the peak flow of the predicted hydrograph in the river channel to the peak of flood intensity in the adjacent floodplains might be of interest. Therefore, in this section, we give insights into the ability of the surrogate approach in reproducing the maximum state of a flood event chronologically.

Fig. 12 shows the expansion of the maximum state of the floods (maximum flow depth within simulation period) over time relative to the time of peak discharge in the modelled hydrographs of the transient model and the synthetic hydrographs of the surrogate model. We see that the evolution of the expansion curve is similar with both approaches, especially for areas that reach maximum state within the first 3 h after the peak.

4. Discussion

Here we discuss the results presented in the previous section regarding the target user groups. Being aware of national/regional differences in the role certain user groups may play, we assume that the three selected are mostly similar for a large fraction of countries. As mentioned, we inferred the needs of the stakeholders from a close collaboration over recent years and emphasize that the definition of their profiles is not in the focus of this study. Nevertheless, we see it as crucial to consider the perspective of the stakeholder in the development of IBW and IF systems, as these systems aim to bridge the communication gap to the stakeholder by responding to their requirements and competences.

4.1. Flood event management of civil protection

Regarding the high responsibility attributed to civil protection (e.g., fire brigades or regionally operating crisis management staffs) during extreme flood events in Switzerland, an adequate warning of this type of stakeholder is of major importance. Warnings triggering wrong action, because, for example, uncertainties are not clearly communicated, might have a major influence in the success of impact mitigation of a flood. We showed that despite only matching peaks of predefined scenarios to hydrographs, surrogate models can represent high resolution transient models with a *Model Fit* of 0.84 for flooded area and 0.89 for exposed people. This means that the loss of information is relatively

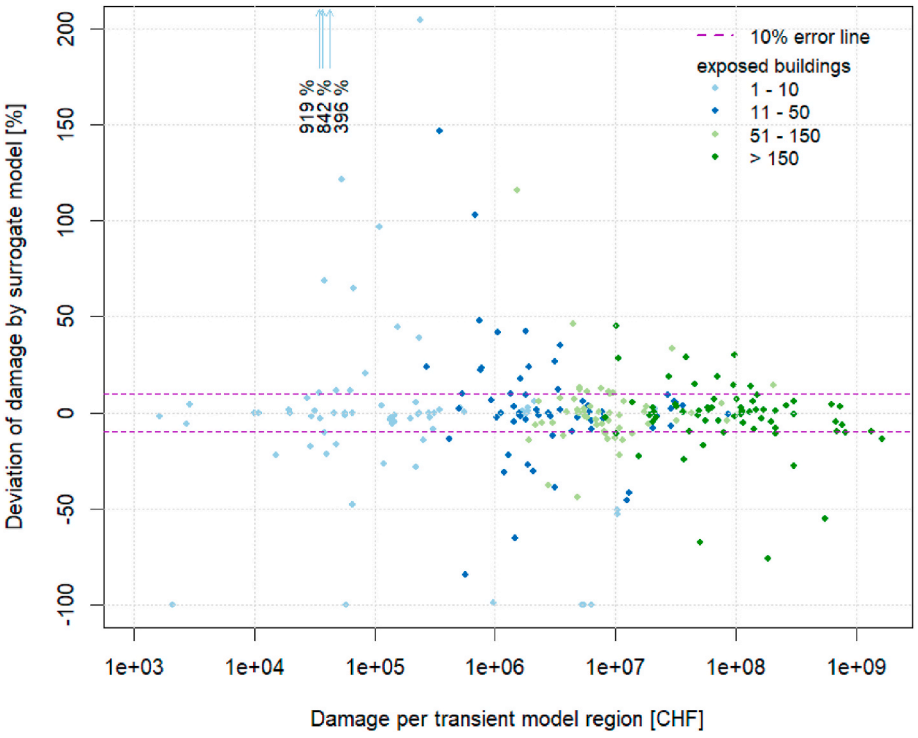

Fig. 11. Relative difference of damage between transient approach and approximation with surrogates. The dots represent one full model region.

modest. Areas where rather high impact is expected (hazard classes 3 and 4), are represented accurately. This is important for civil protection to prioritize endangered regions in the planning of their actions. A visualization of the hazard zones and vulnerable regions on a map, e. g., as presented is crucial for civil protection. We recommend providing multiple maps showing a range of impacts. High computational efficiency was shown by extracting flood surrogate models and combining them with exposure data for impact analysis within minutes, supporting a high potential for an implementation into a warning system.

We also showed that the surrogate model method even provides a good representation of temporal aspects when it comes to predicting the maximum intensity of an event reached in the first hours. As dikes are well represented in both flood models, it also gives a good overview of the sequence of river capacities overtopped along the river reach. We suggest that forwarding temporal information about such weak points should occur where high-resolution models considering geomorphic characteristics of the river channel and especially its dikes are available. As an alternative, the analysis of the expansion of the wet area instead of the maximum flow depth could be interesting as well. The issue with expansion of the wet area is how to consider events that overtop the river capacity with, e. g., two peaks or consisting of two or more phases with intense precipitation (as shown in Fig. 6), where for certain areas the time of exposure to the time of maximum state can be large, which is not covered by the synthetic hydrographs consisting of only one peak. To solve this problem if temporal evolution of wetted area is of interest, the fit of the surrogate should be done also to local maxima of the hydrograph, not only the overall peak.

The surrogate model approach being used to provide hazard maps meets the technical requirements for a web-based solution, but of course also for a locally running system. Storage of the surrogates on a database like PostgreSQL together with PostGIS extension also allows quick cartographical analysis of any precalculated scenario with a GIS.

4.2. Preparing insurance companies on cantonal to national scale

Part of flood mitigation is what comes after an event that caused a lot of damage – cleaning up and restore a similar state as before in a reasonable time, bringing back normal life. For this purpose, insurance companies liquidate money within a short time.

Comparing the transient model and the flood library approach, we saw that especially floodplains with low damage and therefore fewer exposed buildings show the highest relative differences, whereas small relative differences in floodplains with high damage can be very meaningful for the overall loss estimation. In seven out of nine scenarios, the overall relative difference was less than 10%. We recommend considering flood volume and/or the next-to-closest fitting surrogate(s) and thereby having a range of possible outcomes of a predicted scenario to account for uncertainties in terms of monetary damage. Based on a check of a sample of the simulated scenarios, we see that for a considerable fraction of the regions in this study, the damage estimated by the transient model between the two closest fits from the flood surrogate model. We also strongly suggest the application of a validated impact model for every region with different typology of cultural heritage and building characteristics (Zischg et al., 2021).

We emphasize that the definition of the model boundary, uncertainties of the underlying digital elevation model, the selection of the vulnerability function, the resolution of the computational mesh, and the specification of topographic breaklines might have an impact on the estimation on building level. Therefore, it is possible that with the method applied here, in certain cases with single or just a few buildings affected, depending on the flow depth at the building and the size of the footprint, a difference in the damage estimation can result.

4.3. Alerting private persons by warning services

If we look at the number of persons that a warning based on flood surrogate model compared to a transient model is issued, more than 187′500 would receive a warning in both cases, whereas 16′000 would not receive any warning, 8′000 people would be warned without being exposed to the flood. Although the numbers of misses and false alarms seem to be high in absolute terms, the *Model Fit* (0.89) putting them into perspective to the number of hits implies that the accuracy is still good.

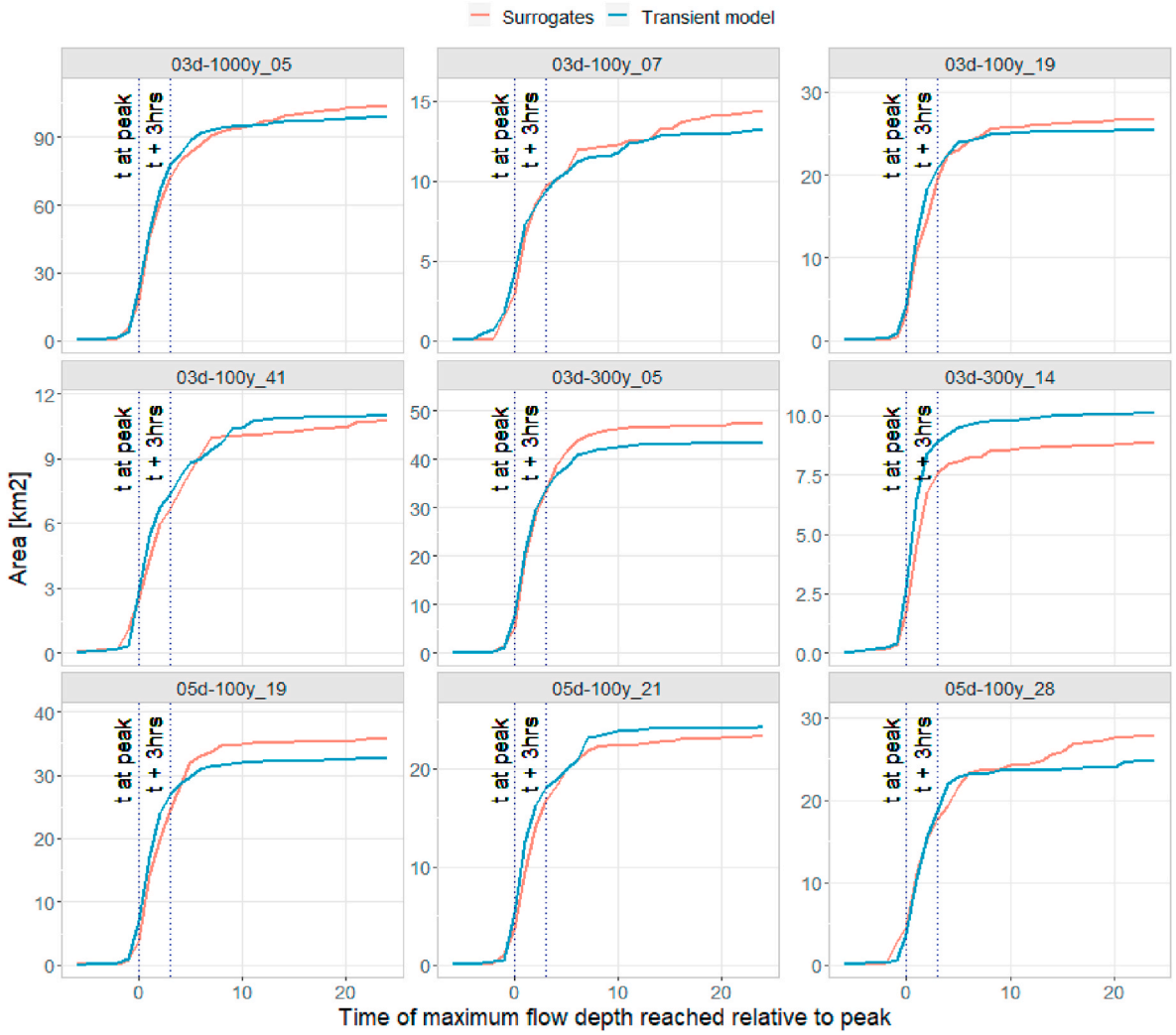

Fig. 12. Expansion of maximum state of floods over time across all modelled regions. The X-axis reflects the time difference (in hours) between the time of maximum flow depth at the element-location and the time when peak-discharge is reached in the river channel (time of maximum flow depth in floodplain minus time of peak-discharge in river channel). The Y-axis shows the flooded area in km^2 reaching maximum state over the whole study region (note that this Y-axis is scaled differently for each scenario). For the naming of the scenarios, see the last paragraph in section 2.4.2. Note that t = 0 is set when the peak discharge is reached (=t at peak), t + 3hrs indicates expansion of the maximum flow depth 3 h after the peak discharge is reached.

The third hazard class represents flood intensities where people outside of buildings (as pedestrians or drivers of a car) are endangered, whereas the fourth hazard class identifies regions/buildings with such intensities that even high damage is expected and probably also a failure of building structures must be assumed to occur. We show that 85–89% of the buildings and persons that are classified with hazard level 3 or 4 by the transient model are attributed with the same hazard level by the surrogate.

These numbers indicate a potential for an implementation of behavioral recommendations in flood warnings. As this was not part of this study, this must be evaluated in further studies. We also highlight that there is a need for studies looking at consequences of false alarms and misses (relative to hits), trying to answer the question of what accuracy is acceptable or even perceived or reputed as good by society, such that there would be no discussions about missed responsibilities (rather in case of missed warnings) and the reliability of warnings would remain high (despite false alarms). Or in other words: how can people be sensitized for uncertainties in modelled forecasts of impacts.

4.4. Limitations, transferability and outlook

In this section, we discuss the limitations of our study, as well as the transferability of our findings to other locations, and provide an outlook for future research. We focus on the results derived by the hydrodynamic (surrogate) flood models.

4.4.1. Limitations

As stated in section 2.2.2, the possibilities to calibrate and validate the hydrodynamic model are limited: The topography from the time of the last large-scale floods in 2005 and 2007, the most recent relevant events for this purpose, is not reflected in our data, as protective measures were implemented on almost all affected rivers between the floods and the measurements for the cross-profiles and digital elevation models. Nevertheless, we checked the plausibility by comparing the model outcomes of all model regions with the official hazard maps and with technical reports on river hydraulics. Zischg et al. (2018b) show that even uncalibrated hydrodynamic models can reach good validation metrics if the river morphology is well represented in the hydraulic models. To some extent, we see our results as not fully dependent on the model validity, as we focus only on the loss of information when replacing a transient model with a surrogate model. The fact that a surrogate flood model better represents a transient model that was calibrated/validated must be further investigated.

Besides this, there are some technical limitations of the flood model

in the study presented. 1) Bridges crossing the rivers of the 1D flood model are not considered hydraulically. At locations where they are limiting the river capacity, significant differences to a potential real event might occur. 2) Besides this, we see missing culverts in the 2D flood model as the most important lacking structures, making the surrogate model as presented a prototype rather than a "ready-to-use" model. By considering these two points, it could serve as supporting tool to test impact-based warning systems. In that regard, we also want to stress that the role of log jam of culverts and collapse of bridges in extreme events as modelled in this study is not clear. 3) The cross-profiles of the rivers are measured approximately every 100m, meaning that sills/small weirs are often not directly considered, resulting in steeper slopes of the riverbed for certain short river sections than it is the case in reality. 4) The 1D model does not consider superelevation occurring, for example, in river bends. In a right turn for example, the water surface elevation at the left embankment might be underestimated by our models and underestimated at the right embankment. 5) Morphological changes of the river channel due to erosion and sedimentation are neglected. These processes are very likely during extreme events and alter the conveyance capacity.

4.4.2. Transferability

The elements of the model chain used to make transient simulations are replaceable by any other method. Our hindcast events can be replaced by any other measurements or forecast meeting the requirements of the successive hydrological model, which is replaceable itself. The coupled 1D-2D hydraulic model can be exchanged with any other hydraulic model.The advantage of the 1D-2D coupled flood model from BASEMENT is that a major part of the preprocessing steps can be automated just based on cross-section point data, 2D model perimeters, breaklines defining relevant hydraulic structures like dams in the floodplain and lines defining the coupling interface of the 1D and 2D model. In addition, the model runs can be initiated via batch process and allow for parallel computing. The framework of the surrogate flood model is transferable to any location where appropriate data is available.

4.4.3. Outlook

Besides overcoming the major limitations mentioned above by including bridges and culverts into the hydrodynamic model, solving the systematic underestimation of the flood volume is required to transfer the prototype to operationalization. Besides the issue that a hydrograph with multiple peaks cannot be mapped by synthetic hydrographs with one peak, and the issue of general differences between volume in synthetic and modelled/forecasted hydrographs based on meteorological data, there is another reason for the underestimation of the volume. The simulation time during the recession phase of the hydrograph determines the flooded area. In diffluent, large floodplains (e. g., Burgdorf) the flood water is covering a larger area the longer the simulation time is. The statistical background of the methodology used to create synthetic hydrographs allows to create alternative scenarios with more/less flood volume with the same peak discharge. Hence, alternative flood peak-flood volume relationships should be implemented in the precalculated scenarios. To solve the volume issues, machine learning techniques as presented by Bentivoglio et al. (2022) could improve the quality of the surrogate model, and probably reduce over- and underestimation issues. Simulations as used in our study could serve as basis to train such a model that might especially be beneficial in model regions with large floodplains, where the preprocessing of scenarios with different flood volumes is costly. Nevertheless, existing studies on local and regional level show issues in generalizing ML-based flood models across different case studies and regions (Bentivoglio et al., 2022).

Due to the good performance of the surrogate model approach, we also see the potential that hydrometeorological uncertainties might be considered by either analyzing multiple members or the range of peaks from the ensemble. Alternatively, increasing k in the k-nearest neighbor analysis could also be used to account for such uncertainties. Here, k could be chosen by the difference of peak discharge from one precalculated scenario to another together with the width of the uncertainty band of a hydrological forecast. Our analyses based on the next-to closest fit shows that the nearest neighbor is generally the better choice, but its consideration can also be beneficial in certain cases. Similar to the volume issue mentioned above, machine learning approaches could help to interpolate between hydrodynamic simulations.

Finally, the issue discussed with the example of the Thur River near Frauenfeld could also be solved by the surrogate model itself: The attenuation effect along a river could be derived in the preprocessing step by documenting the attenuation effect. Additional to the input peak discharge of a synthetic hydrograph, the output peak discharge at the downstream boundary could be measured and entered into the database as well. By applying the surrogate in a downstream direction, the attenuation of the upstream model region could be transmitted to subsequent river reaches and the forecast of the hydrological model could be reduced accordingly.

5. Conclusions

The aim of this study was to evaluate whether computationally fast flood surrogate models can replace computationally heavy transient high-resolution models for near real-time warning applications. For this we compared damage simulations run with flood surrogate models with transient high-resolution models for nine extreme weather scenarios in the north alpine part of Switzerland. We evaluated the following variables: flooded area, flood volume, number of exposed buildings, persons, and workplaces.

Over all scenarios and 78 model regions, the *Model Fits* range from 0.81 (flood volume) to 0.92 (workplaces). The surrogates underestimate monetary damage on average by 7%, showing the potential to warn e. g., (re-) insurance companies of losses.

Flood surrogate models can support intervention forces during an event: 89% of exposed persons in the transient model are similarly classified by the surrogate model. There is also a satisfying representation of the temporal evolution of the maximum flow depth by the surrogates. Hazard maps derived from the surrogates indicate regions where people might be exposed to a high risk of life. By using the surrogate model approach, multiple scenarios can be efficiently analyzed (and mapped) to account for uncertainties.

However, we compare two models at magnitudes where very limited observational validation is possible. We used synthetic hydrographs with single peaks to create scenarios for the flood surrogate models. If the discharge volume above river capacity substantially differs from a forecasted hydrograph, the expansion of floods in diffluent floodplains or the magnitude reached in retention areas in the surrogate should be considered with caution.

Nevertheless, we conclude that flood surrogate models is a valid method to be considered for an application in IBW- and IF-systems, as it optimizes the trade-off between high spatial resolution and computational efficiency: The spatial resolution of the transient model is preserved in the surrogate models and the precalculated flood scenarios, together with exposure data, can be derived, processed and aggregated to stakeholder specific needs for multiple scenarios quasi real-time.

Software & data availability

The transient simulations can be viewed and interactively queried at https://flooddynamics.floodrisk.ch. The original source code of hydrological model "DECIPHeR Dynamic fluxEs and ConnectIvity for Predictions of HydRology" is freely available at https://github.com/uob-hydrology/DECIPHeR; the code version applied in this study is available upon request (please contact M. Kauzlaric by writing to martina.kauzlaric@unibe.ch). The hydrodynamic model BASEMENT-ETHZ is available at https://basement.ethz.ch/. The exposure data can be viewed in an

aggregated form at https://schadenpotenzial.hochwasserrisiko.ch. We used a PostgreSQL-database (https://www.postgresql.org/, v. 10.17) with PostGIS extension (https://postgis.net/, v. 2.4.4) together with the free software environment of R (https://www.r-project.org/) for accessing and storing data. We do not provide the data used for the flood surrogate model as it is stored on a complex relational database. Due to confidential reasons, we're not allowed to share data of persons and workplaces. The building footprints used in this study can be accessed via the website of the Federal Office of Topography swisstopo (SwissTLM3D, https://www.swisstopo.admin.ch/en/geodata/landscape/tlm3d.html, v. 1.9)

CRediT authorship contribution statement

Markus Mosimann: Conceptualization, Data curation, Formal analysis, Methodology, Software, Validation, Visualization, Writing – original draft, Writing – review & editing. **Martina Kauzlaric:** Data curation, Formal analysis, Methodology, Validation, Writing – original draft, Writing – review & editing. **Simon Schick:** Data curation, Formal analysis, Methodology, Validation, Writing – original draft, Writing – review & editing. **Olivia Martius:** Project administration, Supervision, Writing – original draft, Writing – review & editing. **Andreas Paul Zischg:** Conceptualization, Methodology, Project administration, Supervision, Writing – original draft, Writing – review & editing.

Declaration of competing interest

The authors declare that they have no known competing financial interests or personal relationships that could have appeared to influence the work reported in this paper.

Data availability

I have shared the information about data and software availability in the manuscript

Appendix A. Densities of Model Fits for area (top) and volume (bottom) per region

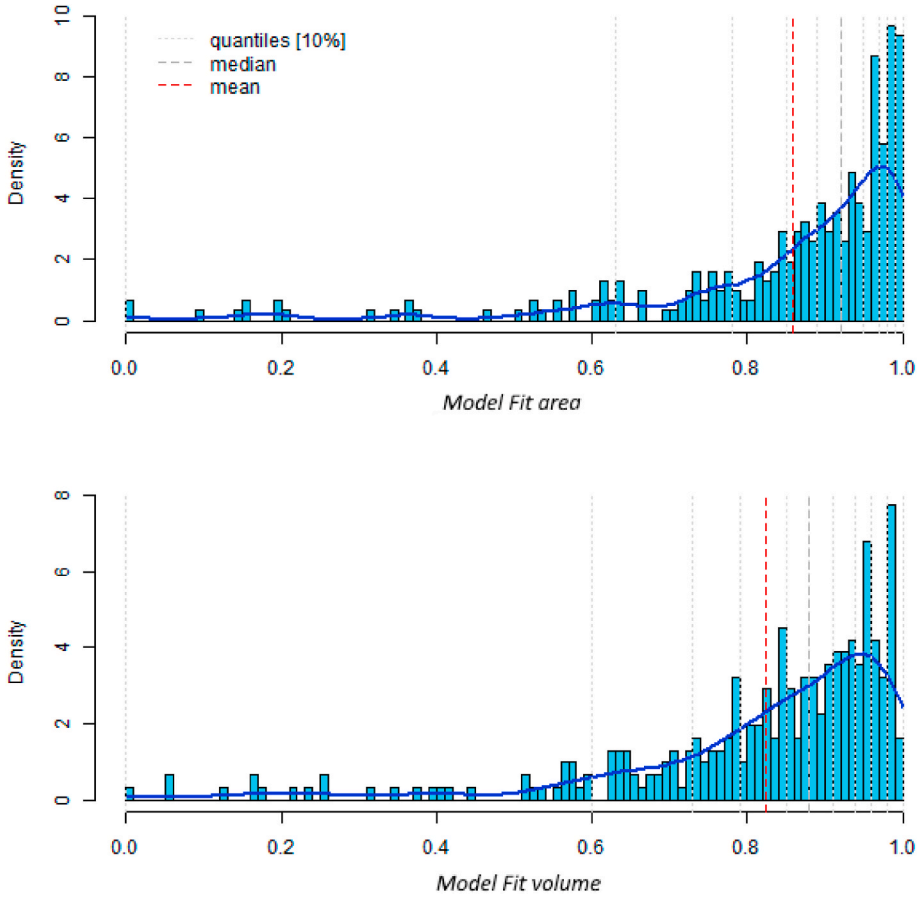

Fig. A. Density distribution of Model Fits for area (top) and volume (bottom) for all regions and scenarios. 10% quantile locations are indicated by the dotted grey lines, the dashed grey line indicates the location of the median (area: 0.92, volume: 0.88), the red line shows the location of the mean (area: 0.86, volume: 0.82).

Appendix B. Goodness of fit for calibration and validation of the hydrological model

Table B. Goodness of fit for calibration and validation of the hydrological model. Hydroligcal measurements are provided by the Federal Office for the Environment (FOEN, 2023c).

		cal 2005–2007					val 2008–2010				
River	Location	*NSE*	*KGE2009*	*PBIAS*	*biasSFMS*	*biasFDChigh*	*NSE*	*KGE2009*	*PBIAS*	*biasSFMS*	*biasFDChigh*
Rhein	Domat/Ems	0.058	0.486	−33.955	−0.280	−0.222	0.247	0.522	−41.431	−0.248	−0.260
Aare	Thun	*0.862*	*0.909*	*−3.132*	*−0.013*	*0.044*	*0.795*	*0.877*	*−7.421*	*0.011*	*−0.005*
Reuss	Luzern	0.903	0.948	−1.652	−0.044	0.013	0.890	0.942	0.041	0.034	0.017
Thur	Andelfinden	0.751	0.861	2.305	−0.021	−0.022	0.665	0.818	8.144	−0.040	0.018
Linth	Weesen	0.803	0.866	−8.942	−0.014	−0.046	0.888	0.875	0.304	0.076	0.063
Emme	Wiler	0.665	0.727	21.058	0.107	0.184	0.522	0.712	10.794	0.169	0.035
Birs	Muenchenstein	0.733	0.848	7.571	−0.014	0.021	0.434	0.675	0.166	−0.160	−0.111
Kleine Emme	Emmen	0.786	0.858	8.707	0.023	0.048	0.688	0.783	14.841	0.288	0.127
Wigger	Zofingen	0.523	0.585	37.535	0.308	0.246	0.382	0.619	29.868	0.027	0.109
Toess	Neftenbach	0.672	0.827	6.363	0.003	0.058	0.674	0.784	0.739	−0.087	−0.067
Doubs	Ocourt	0.376	0.616	−18.945	−0.147	−0.125	0.028	0.456	−25.189	−0.330	−0.187
Broye	Vully-les-Lacs	0.545	0.704	−10.730	−0.110	−0.162	0.388	0.345	−30.798	−0.329	−0.393

Appendix C. Signals and calculated metrics per scenario

		03d-1000y_05	03d-100y_07	03d-100y_19	03d-100y_41	03d-300y_05	03d-300y_14	05d-100y_19	05d-100y_21	05d-100y_28	OVERALL
Hits	*Area [km^2]*	98.514	13.539	22.337	10.456	41.77	8.749	30.217	22.484	26.52	**274.586**
	Volume [mio m^3]	62.329	7.742	16.557	6.447	27.53	6.585	20.568	13.505	15.128	**176.391**
	Buildings	17'413	2'117	2'705	2'281	5'223	1'952	3'728	3'995	4'926	**44'340**
	Persons	74'831	8'553	10'682	9'891	20'742	9'420	14'292	16'567	23'861	**188'839**
	Employees	93'617	21'206	8'880	14'961	29'347	8'689	12'698	22'086	46'367	**257'851**
False Alarms	*Area [km^2]*	6.184	1.094	4.425	0.326	6.644	0.111	5.727	0.815	2.27	**27.596**
	Volume [mio m^3]	3.566	0.978	3.127	0.243	5.202	0.263	4.051	1.204	1.907	**20.541**
	Buildings	862	185	115	136	201	24	129	109	238	**1'999**
	Persons	3'022	1'885	247	511	355	58	132	473	911	**7'594**
	Employees	2'268	1'135	696	1'126	232	437	573	284	1'285	**8'036**
Misses	*Area [km^2]*	5.956	1.039	3.464	0.81	3.294	1.688	3.557	2.171	1.546	**23.525**
	Volume [mio m^3]	7.08	0.657	2.374	0.502	3.387	0.576	2.884	1.627	1.51	**20.597**
	Buildings	1'061	54	360	163	604	742	707	254	262	**4'207**
	Persons	3'617	60	1'480	179	2'721	2'763	2'730	898	735	**15'183**
	Employees	4'265	96	927	919	3'976	1'615	1'473	436	565	**14'272**
FAI	*Area*	0.89	0.86	0.74	0.90	0.81	0.83	0.76	0.88	0.87	**0.84**
	Volume	0.85	0.83	0.75	0.90	0.76	0.89	0.75	0.83	0.82	**0.81**
	Buildings	0.90	0.90	0.85	0.88	0.87	0.72	0.82	0.92	0.91	**0.88**
	Persons	0.92	0.81	0.86	0.93	0.87	0.77	0.83	0.92	0.94	**0.89**
	Employees	0.93	0.95	0.85	0.88	0.87	0.81	0.86	0.97	0.96	**0.92**
BIAS	*Area*	1.002	1.004	1.037	0.957	1.074	0.849	1.064	0.945	1.026	**1.014**
	Volume	0.949	1.038	1.040	0.963	1.059	0.956	1.050	0.972	1.024	**1.000**
	Buildings	0.989	1.060	0.920	0.989	0.931	0.733	0.870	0.966	0.995	**0.955**
	Persons	0.992	1.212	0.899	1.033	0.899	0.778	0.847	0.976	1.007	**0.963**
	Employees	0.980	1.049	0.976	1.013	0.888	0.886	0.936	0.993	1.015	**0.977**

Table C. Signals and calculated metrics per scenario and exposure variable. *BIAS* and *Model Fit* are both optimized at 1 (highlighted with green color).

Appendix D. Scenario specific differences in Model Fits between the two nearest neighbors

Table D

Difference between scenario-specific Model Fits when using the nearest neighbor (k = 1) and the next-to closest fit (k = 2). Differences are calculated by subtracting the Model Fits based on k = 1 from the Model Fits based on k = 2. Hence, negative (blueish) values indicate that the nearest neighbor better represents the transient flood simulation than the next-to closest fit, positive (reddish) values show that for the specific scenario, the selection of the next-to closest fit would have been the better choice.

Scenario	DELTA *Model Fit* (*Model Fit* K2 - *Model Fit* K1) Area	Buildings	Persons	Workplaces
03d-1000y_05	-0.03	-0.01	-0.01	-0.01
03d-100y_07	-0.05	-0.09	0.02	-0.11
03d-100y_19	0.05	-0.04	-0.03	-0.19
03d-100y_41	-0.07	-0.08	-0.12	-0.03
03d-300y_05	-0.05	-0.03	-0.02	0.03
03d-300y_14	-0.02	0.06	0.04	-0.01
05d-100y_19	-0.05	-0.03	-0.04	-0.17
05d-100y_21	-0.10	-0.08	-0.08	-0.28
05d-100y_28	0.01	-0.03	-0.05	-0.04

References

Aargau, Kanton, 2014. DTM 0.5-Meter Raster.

Aldridge, Timothy, Gunawan, Oliver, Moore, Robert J., Cole, Steven J., Boyce, Graeme, Cowling, Rob, 2020. Developing an impact library for forecasting surface water flood risk. J Flood Risk Management 13 (3). https://doi.org/10.1111/jfr3.12641.

Alfieri, Lorenzo, Feyen, Luc, Salamon, Peter, Thielen, Jutta, Bianchi, Alessandra, Dottori, Francesco, Burek, Peter, 2016. Modelling the socio-economic impact of river floods in Europe. Nat. Hazards Earth Syst. Sci. 16 (6), 1401–1411. https://doi.org/10.5194/nhess-16-1401-2016.

Apel, Heiko, Vorogushyn, Sergiy, Merz, Bruno, 2022. Brief communication: impact forecasting could substantially improve the emergency management of deadly floods: case study July 2021 floods in Germany. Nat. Hazards Earth Syst. Sci. 22 (9), 3005–3014. https://doi.org/10.5194/nhess-22-3005-2022.

Arrighi, C., Pregnolato, M., Dawson, R.J., Castelli, F., 2019. Preparedness against mobility disruption by floods. Sci. Total Environ. 654, 1010–1022. https://doi.org/10.1016/j.scitotenv.2018.11.191.

Bennett, Neil D., Croke, Barry F.W., Guariso, Giorgio, Guillaume, Joseph H.A., Hamilton, Serena H., Jakeman, Anthony J., et al., 2013. Characterising performance of environmental models. Environ. Model. Software 40, 1–20. https://doi.org/10.1016/j.envsoft.2012.09.011.

Bentivoglio, Roberto, Isufi, Elvin, Jonkman, Sebastian Nicolaas, Taormina, Riccardo, 2022. Deep Learning Methods for Flood Mapping: A Review of Existing Applications and Future Research Directions.

Bermúdez, María, Zischg, Andreas Paul, 2018. Sensitivity of flood loss estimates to building representation and flow depth attribution methods in micro-scale flood modelling. Nat. Hazards 92 (3), 1633–1648. https://doi.org/10.1007/s11069-018-3270-7.

Bermúdez, María, Ntegeka, Victor, Wolfs, Vincent, Willems, Patrick, 2018. Development and comparison of two fast surrogate models for urban pluvial flood simulations. Water Resour. Manag. 32 (8), 2801–2815. https://doi.org/10.1007/s11269-018-1959-8.

Casteel, Mark A., 2016. Communicating increased risk: an empirical investigation of the national weather service's impact-based warnings. Weather, Climate, and Society 8 (3), 219–232. https://doi.org/10.1175/WCAS-D-15-0044.1.

Casteel, Mark A., 2018. An empirical assessment of impact based tornado warnings on shelter in place decisions. Int. J. Disaster Risk Reduc. 30, 25–33. https://doi.org/10.1016/j.ijdrr.2018.01.036.

Coles, Stuart, 2001. An Introduction to Statistical Modeling of Extreme Values. Springer London, London.

Costabile, Pierfranco, Costanzo, Carmelina, Lorenzo, Gianluca de, Santis, Rosa de, Penna, Nadia, Macchione, Francesco, 2021. Terrestrial and airborne laser scanning and 2-D modelling for 3-D flood hazard maps in urban areas: new opportunities and perspectives. Environ. Model. Software 135, 104889. https://doi.org/10.1016/j.envsoft.2020.104889.

Cox, Tom, Hampson, Rosemary, Hooper, Robert, Hunter, Neil, Porter, I-Hsien, Beatriz, Revilla-Romero, et al., 2021. Real-time flood impacts mapping. Technical report. Environment Agency. Available online at https://assets.publishing.service.gov.uk/media/6037956ae90e070563e5a6da/Real-time_flood_impacts_mapping_-_report_1_.pdf. . (Accessed 28 June 2022). checked on.

Coxon, Gemma, Freer, Jim, Lane, Rosanna, Dunne, Toby, Knoben, Wouter J.M., Howden, Nicholas J.K., et al., 2019. DECIPHeR v1: dynamic fluxEs and ConnectIvity for predictions of HydRology. Geosci. Model Dev. (GMD) 12 (6), 2285–2306. https://doi.org/10.5194/gmd-12-2285-2019.

de Vaud, Canton, 2004. Modèles Altimétriques LiDAR.

Falter, Daniela, Vorogushyn, Sergiy, Lhomme, Julien, Apel, Heiko, Gouldby, Ben, Merz, Bruno, 2013. Hydraulic model evaluation for large-scale flood risk assessments. Hydrol. Process. 27 (9), 1331–1340. https://doi.org/10.1002/hyp.9553.

Falter, Daniela, Schröter, Kai, Dung, Nguyen Viet, Vorogushyn, Sergiy, Kreibich, Heidi, Hundecha, Yeshewatesfa, et al., 2015. Spatially coherent flood risk assessment based on long-term continuous simulation with a coupled model chain. J. Hydrol. 524 (13), 182–193. https://doi.org/10.1016/j.jhydrol.2015.02.021.

Farrag, Mostafa, Brill, Fabio, Dung, Nguyen Viet, Sairam, Nivedita, Schröter, Kai, Kreibich, Heidi, et al., 2022. On the role of floodplain storage and hydrodynamic interactions in flood risk estimation. Hydrol. Sci. J. 67 (4), 508–534. https://doi.org/10.1080/02626667.2022.2030058.

Fekete, Alexander, Sandholz, Simone, 2021. Here comes the flood, but not failure? Lessons to learn after the heavy rain and pluvial floods in Germany 2021. Water 13 (21), 3016. https://doi.org/10.3390/w13213016.

Felder, Guido, Zischg, Andreas, Weingartner, Rolf, 2017. The effect of coupling hydrologic and hydrodynamic models on probable maximum flood estimation. J. Hydrol. 550, 157–165. https://doi.org/10.1016/j.jhydrol.2017.04.052.

Felder, Guido, Gómez-Navarro, Juan José, Zischg, Andreas Paul, Raible, Christoph C., Röthlisberger, Veronika, Bozhinova, Denica, et al., 2018. From global circulation to local flood loss: coupling models across the scales. Sci. Total Environ. 635, 1225–1239. https://doi.org/10.1016/j.scitotenv.2018.04.170.

FOEN, 2023a. Flood alert map for rivers and lakes of national interest. Federal Office for the Environment FOEN. Available online at https://www.hydrodaten.admin.ch/en/warnkarte_national.html. . (Accessed 22 February 2023). updated on 2/22/2023, checked on.

FOEN, 2023b. Naturgefahren: flussvermessung. Federal Office for the environment FOEN. Available online at https://www.bafu.admin.ch/bafu/de/home/themen/naturgefahren/fachinformationen/naturgefahrensituation-und-raumnutzung/gefahrengrundlagen/naturgefahren–flussvermessung.html. . checked on 22.02.23.

FOEN, 2023c. Stations and data. Federal Office for the environment FOEN. Available online at. https://www.hydrodaten.admin.ch/en/stations-and-data.html. (Accessed 22 February 2023). updated on 2/22/2023, checked on.

Foudi, S., Osés-Eraso, N., Tamayo, I., 2015. Integrated spatial flood risk assessment: the case of Zaragoza. Land Use Pol. 42, 278–292. https://doi.org/10.1016/j.landusepol.2014.08.002 (special issue no. 14).

Gabbi, Jeannette, Carenzo, Marco, Pellicciotti, Francesca, Bauder, Andreas, Funk, Martin, 2014. A comparison of empirical and physically based glacier surface melt models for long-term simulations of glacier response. J. Glaciol. 60 (224), 1140–1154. https://doi.org/10.3189/2014JoG14J011.

Horritt, M.S., Bates, P.D., 2002. Evaluation of 1D and 2D numerical models for predicting river flood inundation. J. Hydrol. 268 (1–4), 87–99. https://doi.org/10.1016/S0022-1694(02)00121-X.

Intergovernmental Panel on Climate Change, 2012. Special report of working groups I and II of the intergovernmental Panel on climate change. In: Managing the Risks of Extreme Events and Disasters to Advance Climate Change Adaptation. Cambridge University Press, Cambridge.

Ivanov, Martin A., Kotlarski, Sven, 2017. Assessing distribution-based climate model bias correction methods over an alpine domain: added value and limitations. Int. J. Climatol. 37 (5), 2633–2653. https://doi.org/10.1002/joc.4870.

Johnson, Stephanie J., Stockdale, Timothy N., Ferranti, Laura, Balmaseda, Magdalena A., Molteni, Franco, Magnusson, Linus, et al., 2019. SEAS5: the new ECMWF seasonal forecast system. Geosci. Model Dev. (GMD) 12 (3), 1087–1117. https://doi.org/10.5194/gmd-12-1087-2019.

Kaltenberger, Rainer, Schaffhauser, Andreas, Staudinger, Michael, 2020. "What the weather will do" – results of a survey on impact-oriented and impact-based warnings in European NMHSs. Adv. Sci. Res. 17, 29–38. https://doi.org/10.5194/asr-17-29-2020.

KAWA: LIDAR-Daten Kanton Bern.

Kelder, T., Müller, M., Slater, L.J., Marjoribanks, T.I., Wilby, R.L., Prudhomme, C., et al., 2020. Using UNSEEN trends to detect decadal changes in 100-year precipitation extremes. npj Clim Atmos Sci 3 (1). https://doi.org/10.1038/s41612-020-00149-4.

Kuhn, M., 1987. Micro-meteorological conditions for snow melt. J. Glaciol. 33 (113), 24–26. https://doi.org/10.3189/S002214300000530X.

Luzern, Kanton, 2012. Digitales Terrainmodell (DTM) 2012, 0.5m-Raster.
Mario, Betschart, 2012. A study of convective events in Switzerland with radar and a high-resolution NWP mode. Edited by federal Office of meteorology and climatology, MeteoSwiss. Scientific Report MeteoSwiss 90. Available online at. https://www.meteoswiss.admin.ch/services-and-publications/publications/scientific-publications/2012/a-study-of-convective-events-in-switzerland-with-radar-and-a-high-resolution-nwp-model.html. (Accessed 7 November 2023). checked on.
Meléndez-Landaverde, Erika R., Werner, Micha, Verkade, Jan, 2020. Exploring protective decision-making in the context of impact-based flood warnings. J Flood Risk Management 13 (1). https://doi.org/10.1111/jfr3.12587.
MeteoSwiss, 2017. Hourly Precipitation Estimation through Rain-Gauge and Radar: CombiPrecip. Federal Office of Meteorology and Climatology Meteo Swiss. Available online at file:///C:/Users/mmosimann/Downloads/ProdDoc_CPC.pdf, checked on. (Accessed 7 July 2022).
Ming, Xiaodong, Liang, Qiuhua, Xia, Xilin, Li, Dingmin, Fowler, Hayley J., 2020. Real-time flood forecasting based on a high-performance 2-D hydrodynamic model and numerical weather predictions. Water Resour. Res. 56 (7) https://doi.org/10.1029/2019WR025583.
Moncoulon, D., Labat, D., Ardon, J., Leblois, E., Onfroy, T., Poulard, C., et al., 2014. Analysis of the French insurance market exposure to floods: a stochastic model combining river overflow and surface runoff. Nat. Hazards Earth Syst. Sci. 14 (9), 2469–2485. https://doi.org/10.5194/nhess-14-2469-2014.
Nadarajah, Saralees, 2007. Probability models for unit hydrograph derivation. J. Hydrol. 344 (3–4), 185–189. https://doi.org/10.1016/j.jhydrol.2007.07.004.
NCCS, 2018. CH2018 - climate scenarios for Switzerland, technical report. National Centre for climate services. Zurich. Available online at https://www.nccs.admin.ch/nccs/en/home/data-and-media-library/data/ch2018—climate-scenarios-for-switzerland.html. . checked on 7/6/2022.
Neal, J., Schumann, G., Fewtrell, T., Budimir, M., Bates, P., Mason, D., 2011. Evaluating a new LISFLOOD-FP formulation with data from the summer 2007 floods in Tewkesbury, UK. J Flood Risk Management 4 (2), 88–95. https://doi.org/10.1111/j.1753-318X.2011.01093.x.
Neal, Jeffrey, Schumann, Guy, Bates, Paul, 2012. A subgrid channel model for simulating river hydraulics and floodplain inundation over large and data sparse areas. Water Resour. Res. 48 (11), 619. https://doi.org/10.1029/2012WR012514.
Neal, Jeffrey C., Odoni, Nicholas A., Trigg, Mark A., Freer, Jim E., Garcia-Pintado, Javier, Mason, David C., et al., 2015. Efficient incorporation of channel cross-section geometry uncertainty into regional and global scale flood inundation models. J. Hydrol. 529, 169–183. https://doi.org/10.1016/j.jhydrol.2015.07.026.
Panziera, L., Gabella, M., Germann, U., Martius, O., 2018. A 12-year radar-based climatology of daily and sub-daily extreme precipitation over the Swiss Alps. Int. J. Climatol. 38 (10), 3749–3769. https://doi.org/10.1002/joc.5528.
Potter, Sally, Harrison, Sara, Kreft, Peter, 2021. The benefits and challenges of implementing impact-based severe weather warning systems: perspectives of weather, flood, and emergency management personnel. Weather, Climate, and Society 13 (2), 303–314. https://doi.org/10.1175/WCAS-D-20-0110.1.
Pregnolato, Maria, Ford, Alistair, Wilkinson, Sean M., Dawson, Richard J., 2017. The impact of flooding on road transport: a depth-disruption function. Transport. Res. Transport Environ. 55, 67–81. https://doi.org/10.1016/j.trd.2017.06.020.
Rai, R.K., Sarkar, S., Singh, V.P., 2009. Evaluation of the adequacy of statistical distribution functions for deriving unit hydrograph. Water Resour. Manag. 23 (5), 899–929. https://doi.org/10.1007/s11269-008-9306-0.
Razavi, Saman, Tolson, Bryan A., Burn, Donald H., 2012. Review of surrogate modeling in water resources. Water Resour. Res. 48 (7) https://doi.org/10.1029/2011WR011527.
RPF, 2015. Hydraulische Berechnungen Hochrhein.
Russo, Beniamino, Sunyer, David, Velasco, Marc, Djordjević, Slobodan, 2015. Analysis of extreme flooding events through a calibrated 1D/2D coupled model: the case of Barcelona (Spain). J. Hydroinf. 17 (3), 473–491. https://doi.org/10.2166/hydro.2014.063.
Serinaldi, Francesco, Grimaldi, Salvatore, 2011. Synthetic design hydrographs based on distribution functions with finite support. J. Hydrol. Eng. 16 (5), 434–446. https://doi.org/10.1061/(ASCE)HE.1943-5584.0000339.
Shannon, Sarah, Payne, Anthony, Freer, Jim, Coxon, Gemma, Kauzlaric, Martina, Kriegel, David, Harrison, Stephan, 2023. A snow and glacier hydrological model for large catchments – case study for the Naryn River, central Asia. Hydrol. Earth Syst. Sci. 27 (2), 453–480. https://doi.org/10.5194/hess-27-453-2023.
Sideris, I.V., Gabella, M., Erdin, R., Germann, U., 2014. Real-time radar-rain-gauge merging using spatio-temporal co-kriging with external drift in the alpine terrain of Switzerland. Q. J. R. Meteorol. Soc. 140 (680), 1097–1111. https://doi.org/10.1002/qj.2188.
Solothurn, Kanton, 2014. Digitales Terrainmodell (DTM) 2014.
Stockdale, Tim, 2021. SEAS5 User Guide. European Centre for Medium-Range Weather Forecasts. Swisstopo (2013): SwissALTI3D. Federal Office of Topography, Swisstopo. Available online at. https://shop.swisstopo.admin.ch/de/products/height_models/alti3D. checked on 5/16/2017. swisstopo (2023): National Map 1:10 000.
swisstopo, 2013. SwissALTI3D. Federal Office of Topography, swisstopo. Available online at https://www.swisstopo.admin.ch/en/geodata/height/alti3d.html, checked on 01/10/2024.
swisstopo, 2023. Swiss Map Raster 10. Available online at https://www.swisstopo.admin.ch/de/geodata/maps/smr/smr10.html, checked on 01/10/2024.
Thompson, Vikki, Dunstone, Nick J., Scaife, Adam A., Smith, Doug M., Slingo, Julia M., Brown, Simon, Belcher, Stephen E., 2017. High risk of unprecedented UK rainfall in the current climate. Nat. Commun. 8 (1), 107. https://doi.org/10.1038/s41467-017-00275-3.
United Nations, 2015. Sendai Framework for Disaster Risk Reduction 2015-2030. United Nations Office for Disaster Risk Reduction. Available online at Sendai Framework for Disaster Risk Reduction 2015-2030, updated on 3/18/2015, checked on 6/24/2022.
van Dyck, Jozef, Willems, Patrick, 2013. Probabilistic flood risk assessment over large geographical regions. Water Resour. Res. 49 (6), 3330–3344. https://doi.org/10.1002/wrcr.20149.
Vetsch, D., Siviglia, A., Caponi, F., Ehrbar, D., Gerke, E., Kammerer, S., et al., 2018. BASEMENT - Basic Simulation Environment for Computation of Environmental Flow and Natural Hazard Simulation. © ETH Zürich, VAW. Version 2.8.
Viviroli, Daniel, Sikorska-Senoner, Anna E., Evin, Guillaume, Staudinger, Maria, Kauzlaric, Martina, Chardon, Jérémy, et al., 2022. Comprehensive space–time hydrometeorological simulations for estimating very rare floods at multiple sites in a large river basin. Nat. Hazards Earth Syst. Sci. 22 (9), 2891–2920. https://doi.org/10.5194/nhess-22-2891-2022.
Ward, Philip J., Jongman, Brenden, Weiland, Frederiek Sperna, Bouwman, Arno, van Beek, Rens, Bierkens, Marc F.P., et al., 2013. Assessing flood risk at the global scale: model setup, results, and sensitivity. Environ. Res. Lett. 8 (4), 44019 https://doi.org/10.1088/1748-9326/8/4/044019.
Wahl, Sabrina, Bollmeyer, Christoph, Crewell, Susanne, Figura, Clarissa, Friederichs, Petra, Hense, Andreas, Keller, Jan D., Ohlwein, Christian, 2017. A novel convective-scale regional reanalysis COSMO-REA2: Improving the representation of precipitation. Metz 26 (4), 345–361. https://doi.org/10.1127/metz/2017/0824.
Weyrich, Philippe, Scolobig, Anna, Bresch, David N., Patt, Anthony, 2018. Effects of impact-based warnings and behavioral recommendations for extreme weather events. Weather, Climate, and Society 10 (4), 781–796. https://doi.org/10.1175/WCAS-D-18-0038.1.
World Meteorological Organization, 2015. WMO guidelines on multi-hazard impact-based forecast and warning services (WMO-No. 1150). Available online at. https://library.wmo.int/doc_num.php?explnum_id=7901. (Accessed 16 September 2021). checked on.
Zischg, Andreas Paul, 2023. Modeling spatiotemporal dynamics of flood risk change. In: Zischg, Andreas (Ed.), Flood Risk Change. A Complexity Perspective. Elsevier, Amsterdam, pp. 187–271.
Zischg, Andreas Paul, Felder, Guido, Mosimann, Markus, Röthlisberger, Veronika, Weingartner, Rolf, 2018a. Extending coupled hydrological-hydraulic model chains with a surrogate model for the estimation of flood losses. Environ. Model. Software 108, 174–185. https://doi.org/10.1016/j.envsoft.2018.08.009.
Zischg, Andreas Paul, Mosimann, Markus, Bernet, Daniel Benjamin, Röthlisberger, Veronika, 2018b. Validation of 2D flood models with insurance claims. J. Hydrol. 557, 350–361. https://doi.org/10.1016/j.jhydrol.2017.12.042.
Zischg, Andreas Paul, Röthlisberger, Veronika, Mosimann, Markus, Profico-Kaltenrieder, Rahel, Bresch, David, Fuchs, Sven, et al., 2021. Evaluating targeted heuristics for vulnerability assessment in flood impact model chains. J Flood Risk Management 5 (10), 171. https://doi.org/10.1111/jfr3.12736.
Zug, Kanton, 2013. Höhenmodell der amtlichen Vermessung 2013 auf Basis "LIDAR.
Zürich, Kanton, 2014. Digitales Terrainmodell (DTM) - 2014.